Acetylation of conserved lysines fine-tunes mitochondrial malate dehydrogenase activity in land plants

Manuel Balparda[1,†] (iD), Marlene Elsässer[2,3,†], Mariana B. Badia[4,5,†] (iD), Jonas Giese[6] (iD), Anastasiia Bovdilova[4],
Meike Hüdig[1,4] (iD), Lisa Reinmuth[2], Jürgen Eirich[6] (iD), Markus Schwarzländer[3] (iD), Iris Finkemeier[6]* (iD),
Mareike Schallenberg-Rüdinger[2]* (iD) and Veronica G. Maurino[1,4]* (iD)

[1]Molecular Plant Physiology, University of Bonn, Kirschallee 1, 53115, Bonn, Germany,

[2]Molecular Evolution, Institute for Cellular and Molecular Botany (IZMB), University of Bonn, Kirschallee 1, 53115, Bonn,
Germany,

[3]Plant Energy Biology, Institute of Plant Biology and Biotechnology (IBBP), University of Münster, Schlossplatz 8, 48143
Münster, Germany,

[4]Plant Molecular Physiology and Biotechnology, Institute of Developmental and Molecular Biology of Plants, Heinrich Heine
University, and Cluster of Excellence on Plant Sciences (CEPLAS), 40225 Düsseldorf, Germany,

[5]Facultad de Química e Ingeniería del Rosario, Pontificia Universidad Católica Argentina, Av. Pellegrini 3314, S2002QEO
Rosario, Argentina, and

[6]Plant Physiology, Institute of Plant Biology and Biotechnology (IBBP), University of Münster, Schlossplatz 7, 48149 Münster,
Germany

SUMMARY

Plants need to rapidly and flexibly adjust their metabolism to changes of their immediate environment. Since this necessity results from the sessile lifestyle of land plants, key mechanisms for orchestrating central metabolic acclimation are likely to have evolved early. Here, we explore the role of lysine acetylation as a post-translational modification to directly modulate metabolic function. We generated a lysine acetylome of the moss *Physcomitrium patens* and identified 638 lysine acetylation sites, mostly found in mitochondrial and plastidial proteins. A comparison with available angiosperm data pinpointed lysine acetylation as a conserved regulatory strategy in land plants. Focusing on mitochondrial central metabolism, we functionally analyzed acetylation of mitochondrial malate dehydrogenase (mMDH), which acts as a hub of plant metabolic flexibility. In *P. patens* mMDH1, we detected a single acetylated lysine located next to one of the four acetylation sites detected in *Arabidopsis thaliana* mMDH1. We assessed the kinetic behavior of recombinant *A. thaliana* and *P. patens* mMDH1 with site-specifically incorporated acetyl-lysines. Acetylation of *A. thaliana* mMDH1 at K169, K170, and K334 decreases its oxaloacetate reduction activity, while acetylation of *P. patens* mMDH1 at K172 increases this activity. We found modulation of the malate oxidation activity only in *A. thaliana* mMDH1, where acetylation of K334 strongly activated it. Comparative homology modeling of MDH proteins revealed that evolutionarily conserved lysines serve as hotspots of acetylation. Our combined analyses indicate lysine acetylation as a common strategy to fine-tune the activity of central metabolic enzymes with likely impact on plant acclimation capacity.

Keywords: protein acetylation, post-transcriptional, regulation, mitochondria, metabolism, malate dehydrogenase.

INTRODUCTION

Flux through central metabolism is particularly dynamic in plants and can change dramatically in response to changes in external conditions or intrinsic demands. For instance, the tricarboxylic acid (TCA) cycle, which takes place in the mitochondria, can operate in a cyclic or non-cyclic mode depending on cell type and the demands for reducing power, ATP, and carbon skeletons (Sweetlove et al., 2010). Although glycolysis-derived pyruvate decarboxylation is considered to be the major entry point for carbon into the TCA cycle in most organisms, in green plant tissues it is

malate rather than pyruvate that acts as the main substrate for the TCA cycle under most circumstances (Sweetlove et al., 2010). Mitochondrial malate dehydrogenase (mMDH; EC 1.1.1.37) interconverts malate and oxaloacetate (OAA) using NAD^+/NADH as co-substrate. *In vivo*, the direction of the reaction depends on the demands of the cells and the redox state of the NAD pool in the matrix (Figure 1). Apart from its classical role in supporting the TCA cycle flux to generate OAA from malate for respiration, mMDH provides OAA for the synthesis of aspartate and – indirectly – of citrate as precursor for nitrogen assimilation (Figure 1) (Hanning and Heldt, 1993; Sweetlove et al., 2010). In particular in illuminated leaves, mMDH can also support metabolic flux in the opposite direction to oxidize NADH to NAD^+ for consumption by the photorespiratory glycine decarboxylase (Journet et al., 1981) and as part of the mitochondrial malate valve that connects the redox states of the NAD pools of the mitochondrial matrix and the cytosol through the exchange of malate and OAA (Figure 1) (Scheibe, 2004; Scheibe et al., 2005; Sweetlove et al., 2010). All these aspects of mitochondrial metabolism are supported by models obtained through diel flux balance analysis (Shameer et al., 2019).

Two isoforms, mMDH1 (AT1G53240) and mMDH2 (AT3G15020), are expressed in *Arabidopsis thaliana*, of which mMDH1 is the main isoform in green tissue (Hüdig et al., 2015; Tomaz et al., 2010). While the *in vivo* mMDH oligomerization state in plants is not yet definitively established, pig heart mMDH is active as a homodimer of approximately 70 kDa, possessing two equivalent binding sites (Gleason et al., 1994; Murphey et al., 1967; Noyes et al., 1974; Shore and Chakrabarti, 1976). Mitochondrial malate is not only metabolized through mMDH, but also via the NAD-dependent malic enzyme (NAD-ME) (Maurino

and Engqvist, 2015; Sweetlove et al., 2010; Tronconi et al., 2008, 2020). Both enzymes together provide a remarkable degree of flexibility to plant respiratory metabolism, since they are able to supply mitochondrial carbon metabolism with substrate to respire, but also replenish the TCA cycle with carbon skeletons to maintain its function even when carbon skeletons are withdrawn for biosynthesis, for example, of amino acids (Sweetlove et al., 2010). While the positioning of mMDH at a branchpoint of central carbon metabolism of plants and its variable engagement depending on flux mode makes active regulation of mMDH activity particularly likely, relatively little is known about this regulation. Modulation of mMDH activity is not only critical to direct carbon flux either to OAA or pyruvate, but it also has the potential to set the total (photo)respiratory flux by NAD^+ provisioning to glycine decarboxylase; such modulation can additionally uncouple the redox states of the NAD pools of the matrix and the cytosol (Shameer et al., 2019; Sweetlove et al., 2010). Plant mMDH was not found to be redox-regulated through the matrix thioredoxin system. Instead, it is most probably controlled in response to variations in the matrix adenine nucleotide balance, as its *in vitro* activity is lowered by ATP and inhibited by an increase in the ATP/ADP ratio within the physiological range (Yoshida and Hisabori, 2016). Recently, in *A. thaliana* seedlings growing in liquid cultures and harvested at the beginning of the light period, mMDH1 was found to be acetylated at four different lysine residues: K170, K325, K329, and K334 (König et al., 2014a). However, the functional significance of those modifications has not been explored.

Post-translational modifications (PTMs), such as phosphorylation and acetylation, can alter protein functions by affecting protein interactions, subcellular localization, or

Figure 1. Direction of the mitochondrial malate dehydrogenase (mMDH) reaction (red arrow) depending on the metabolic demands of the cells and the NAD redox state of the mitochondrial matrix.
(a) Catabolic mode of the tricarboxylic acid (TCA) cycle.
(b) Provision of oxaloacetate (OAA) for the synthesis of citrate as precursor for nitrogen assimilation.
(c) Provision of OAA for the synthesis of aspartate.
(d) Provision of NAD^+ for the photorespiratory glycine decarboxylase (GDC) and of malate for redox balance between matrix and cytosol (modified from Sweetlove et al., 2010).
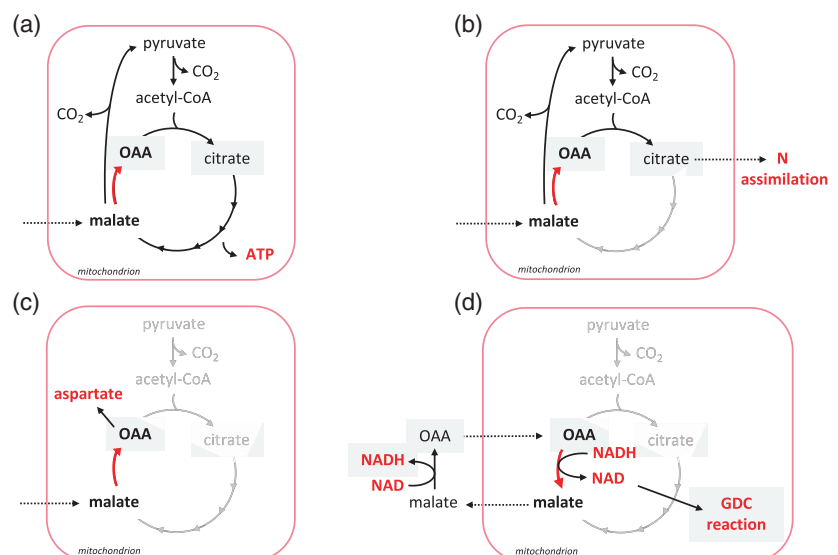
enzymatic activities (Bovdilova et al., 2019; Inuzuka et al., 2012; Matsuzaki et al., 2005; Ventura et al., 2010; Yang and Seto, 2008). Protein acetylation of lysine residues has long been recognized as a regulator of transcriptional control (Allfrey et al., 1964). More recently, this PTM emerged as a regulator of cellular metabolism and signaling in different organisms (Choudhary et al., 2014; Finkemeier et al., 2011; Hansen et al., 2019; König et al., 2014a; Narita et al., 2019; Wang et al., 2010; Zhao et al., 2010).

Lysine acetylation has been found to be particularly widespread in bacterial and mitochondrial proteomes (Weinert et al., 2011; Xu et al., 2009). Two co-enzymes of energy metabolism, acetyl-CoA and NAD^+, are required as substrates for the reversible acetylation of lysine residues (Imai et al., 2000; Lin et al., 2012). Acetyl-CoA is the co-enzyme of lysine acetyltransferases but can also acetylate proteins non-enzymatically at a pH higher than 8 (Guan and Xiong, 2011; Hirschey et al., 2011; König et al., 2014a). NAD^+ is used by sirtuin-type deacetylases, which also reside within mitochondria of mammals (Imai et al., 2000) and plants (König et al., 2014b). In mitochondria, acetyl-CoA and NAD^+ play key roles as metabolic regulators. While acetyl-CoA is produced in the mitochondrial matrix by the pyruvate dehydrogenase complex (PDC) and is oxidized in the TCA cycle, NAD^+ is required as electron acceptor in the TCA cycle. Respiration rates can have a major impact on protein acetylation, since changes in physiological NAD^+ concentration correlate with the activity of sirtuins (Anderson et al., 2017; Lombard et al., 2007). The mitochondrial acetylome of 10-day-old *A. thaliana* seedlings revealed 120 lysine-acetylated proteins, which contained a total of 243 lysine-acetylated sites (König et al., 2014a). Most TCA cycle enzymes of *A. thaliana* were found to be acetylated, which parallels findings in animals and bacteria (König et al., 2014a; Masri et al., 2013; Wang et al., 2010). The fact that the PDC and most of the TCA cycle enzymes were found to be lysine-acetylated across different organisms suggests that acetylation might represent an evolutionarily conserved regulation system for TCA cycle function (Hosp et al., 2017).

Lysine acetylation is overrepresented in both mitochondria and chloroplasts of angiosperm species, suggesting a prominent role of lysine acetylation in the direct modulation of the function of the endosymbiotic organelles (Hartl et al., 2017; Moller et al., 2020). Little is known about the conservation of acetylated lysines in distant land plant species, as investigations of lysine acetylation hitherto covered only flowering plant species (Fang et al., 2015; He et al., 2016; Jiang et al., 2018; König et al., 2014a; Melo-Braga et al., 2012; Smith-Hammond et al., 2014; Zhen et al., 2016).

Here, we used the model moss *Physcomitrium (Physcomitrella) patens* as an early branching land plant (Rensing et al., 2020) to devise a comparative proteomic analysis to shed light on the evolutionary conservation of lysine acetylation in mitochondrial proteins and its potential functional diversification in plants. Our analysis identified lysine acetylation of different mitochondrial proteins of *P. patens*, including mMDH. Using mMDH as a model enzyme of central metabolic importance, we address the question of whether lysine acetylation represents an evolutionarily conserved strategy to modulate mMDH activity. We synthesized *A. thaliana* and *P. patens* acetylated mMDH1 proteoforms at the identified lysine acetylation positions using the genetic code expansion strategy (Neumann et al., 2008), and assessed the kinetic behavior of the recombinant enzyme variants. Our results indicate acetylation of conserved lysines as a common strategy to modulate mitochondrial carboxylic acid metabolism by fine-tuning mMDH activity.

RESULTS

Identification of mitochondrial lysine-acetylated proteins in *P. patens*

To identify lysine-acetylated proteins of the moss *P. patens*, we analyzed its proteome via acetyl-lysine enrichment and liquid chromatography mass spectrometry (LC-MS/MS). The proteome was obtained from gametophores, which represent the haploid and dominant growth stage of mosses, analogous to the sporophyte growth stage of vascular plants (Strotbek et al., 2013). Overall, we detected 6428 protein groups, of which 638 were found to be acetylated on at least one and at most nine lysines (Figure 2; Table S1).

We next classified the identified proteins according to their subcellular localization, making use of a previous analysis of the mitochondrial and plastid proteomes of *P. patens* (Müller et al., 2014). Additional proteins were grouped as organelle-localized when classified as such in the most recent annotation (Lang et al., 2018). In total, 1454 proteins were categorized as organellar proteins, 331 of which were acetylated (Figure 2). Of those, 272 were annotated as plastidial proteins and 98 as mitochondrial, including 39 proteins that were classified as plastidial and/or mitochondrial (Tables S2 and S3). A *post hoc* manual inspection suggested that 16 out of the 98 putative mitochondrial proteins were in fact plastidial (11) or peroxisomal (5; Table S2), and the putative plastidial citrate synthase proteins were rather peroxisomal based on the highest sequence similarity (65–74%) to the peroxisomal citrate synthases of *A. thaliana*. Correcting these misclassifications results in 52 mitochondrial, 30 mitochondrial or plastidial, and 242 plastidial proteins identified as lysine-acetylated (Figure 2).

Similar to previous findings in angiosperms (Hartl et al., 2017; Moller et al., 2020; Smith-Hammond et al., 2014), lysine acetylation is particularly abundant in the
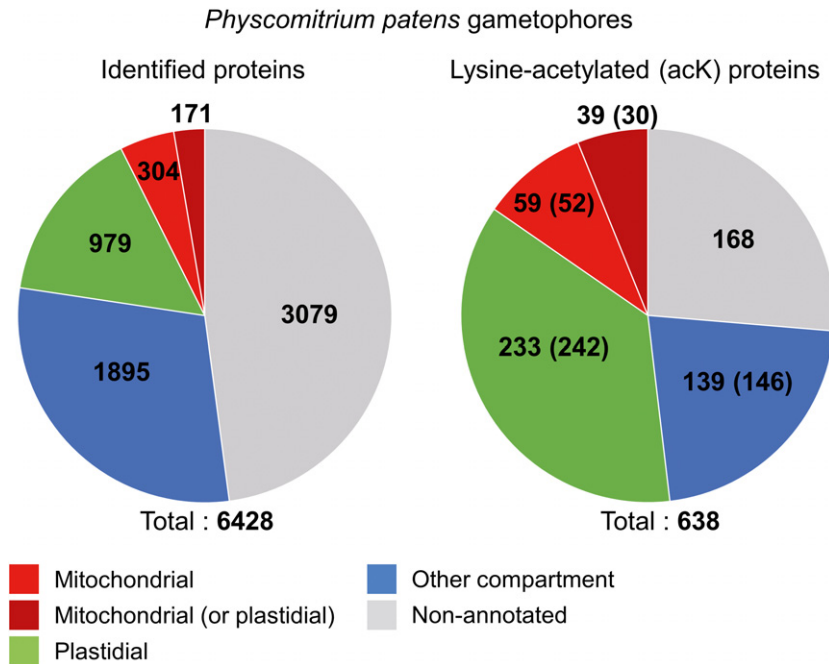
Figure 2. Distribution of lysine acetylation in *Physcomitrium patens* proteins. Displayed are the proteins identified in gametophore samples of *P. patens* (left) and the proteins with detected acetylation sites (right). The proteins are classified as mitochondrial (red), plastidial (green), other compartment (blue), and non-annotated (gray) based on the localization identified in Müller et al. (2014) and the annotation provided by Lang et al. (2018). Proteins which could only be classified as mitochondrial or plastidial are displayed in dark red. Manual inspection suggested different localization for 18 proteins; modified numbers are given in brackets. Organellar proteins are overrepresented in the lysine acetylation dataset ($P < 0.0001$ for equal distribution of acetylation in organellar proteins and non-organellar proteins, statistical significance was tested with the chi-square test using the Excel package XLSTAT [Addinsoft, Paris, France]).

mitochondria and plastids of *P. patens* gametophores. We found that 20% of the identified mitochondrial proteins and 23% of the identified plastidial proteins were acetylated, while only 6% of the other identified proteins possessed this PTM (Figure 2; Table S2). In *P. patens*, we observed lysine acetylation in most TCA cycle enzymes detected in the dataset (aconitase, NAD- and NADP-dependent isocitrate dehydrogenase, 2-oxoglutarate dehydrogenase, and mMDH). This observation mirrors previous results from isolated mitochondria of *A. thaliana* and pea (*Pisum sativum*) seedlings (König et al., 2014a; Smith-Hammond et al., 2014).

Different lysine residues are acetylated in TCA cycle enzymes of *A. thaliana* and *P. patens*

The specific sites of lysine acetylation in TCA cycle enzymes and other mitochondrial proteins were compared between orthologous proteins of *P. patens* and *A. thaliana* (König et al., 2014a). Proteins were clustered into orthologous groups, each consisting of one to six different proteins per species, depending on the number of paralogous proteins encoded in the two genomes and detected in the datasets (Table S1; Table 1). PDC subunit E1α as well as four of the identified TCA cycle enzymes are acetylated in both *P. patens* and *A. thaliana* (Table 1). In contrast, lysine

acetylation of NADP isocitrate dehydrogenase proteins was detected in *P. patens* only (Table S1).

Altogether, we found acetylation of 22 different lysines in the TCA cycle enzymes and PDC subunit E1α in *P. patens* or *A. thaliana*. In 14 of the 22 positions, the lysine, acetylated in one species, was conserved in at least one orthologous protein of the other species. Only PDC subunit E1α and the aconitase of both species shared a lysine that was acetylated in both datasets (Table 1). A similar picture emerged for the other mitochondrial orthologous protein groups investigated (Table S4).

Orthologous proteins of *A. thaliana* and *P. patens* showed conserved lysine positions, but for each individual position, lysine acetylation was typically detected in one of the two species only (Table 1; Table S4).

In addition to the TCA cycle enzymes and the PDC, we classified 25 mitochondrial *A. thaliana* proteins and 31 mitochondrial *P. patens* proteins into 17 further orthologous groups. We found 99 lysine residues to be acetylated in at least one protein of these additional orthologous groups. Of these 99 positions, 66 (67%) carried a lysine in orthologous proteins of the respective other species as well; 12 (12%) of these conserved lysines were acetylated in orthologous proteins of both species (Table S4). Mitochondrial orthologous proteins of *A. thaliana* and *P. patens*

Table 1 Conservation of lysine acetylation between mitochondrial TCA cycle and PDC proteins identified in *Arabidopsis thaliana* and *Physcomitrium patens*

Orthologous protein group	Accession No.	Number of acetylated lysines			Shared lysine acetylation	Position(s) of lysine acetylation site(s)
		Total	Diff	Shared K		
Pyruvate dehydrogenase complex subunit E1α	AT1G24180.1	2	2	1	1	**85**; 336
	AT1G59900.1	2				**81**; 332
	Pp3c12_7580V3.1	1				**86**
	Pp3c4_20210V3.1	1				**86**
Aconitase (TCA)	AT2G05710.1	3	7	5	1	<u>790</u>; 846; 895
	AT4G26970.1	2				<u>795</u>; 900
	Pp3c15_25170V3.1	5				<u>520</u>; <u>529</u>; 598; **<u>803</u>**; 844
	Pp3c9_25990V3.2	2				<u>491</u>; 806
2-Oxoglutarate dehydrogenase E1 (TCA)	AT3G55410.1	3	5	2	0	549; <u>599</u>; 613
	AT5G65750.1	2				<u>603</u>; 873
	Pp3c23_7750V3.1	1				1000
NAD isocitrate dehydrogenase (TCA)	AT3G09810.1	1	3	3	0	<u>181</u>
	AT5G03290.1	2				<u>181</u>; 218
	Pp3c15_3920V3.1	1				<u>365</u>
	Pp3c9_4370V3.1	1				<u>355</u>
Malate dehydrogenase (TCA)	**AT1G53240.1/mMDH1**	4	5	3	0	<u>170</u>; <u>325</u>; <u>329</u>; <u>334</u>
	AT3G15020.1/mMDH2	1				<u>170</u>
	Pp3c4_20940V3.1/MDH1	1				<u>172</u>
	Pp3c12_8120V3.1/mMDH2	1				<u>170</u>
Sum	**AT: 10/Pp: 9**	36	22	14	2	

Proteins identified to be lysine-acetylated in *P. patens* and *A. thaliana* are organized into orthologous groups. Total numbers of identified acetylated lysines (Ks, total), number of acetylated Ks at different positions in the orthologous proteins (diff), numbers of acetylated Ks with conserved lysines at the same position of at least one putative ortholog of the other species (shared K), and shared acetylated lysines are listed separately. Positions of the acetylated lysines in the proteins are given, and numbers are underlined when Ks are conserved in the putative orthologs at this position. Bold numbers represent acetyated lysines which were detected in at least one *P. patens* and one *A. thaliana* putative ortholog of both datasets. Pp, *P. patens*; AT, *A. thaliana*. PDC, pyruvate dehydrogenase complex; TCA, tricarboxylic acid.

showed 66% conserved lysine positions (80/121 positions), which were found to be acetylated in at least one of the orthologs compared in this study. For each individual position, however, lysine acetylation was typically detected in one of the two species only (Table 1; Table S4).

Arabidopsis thaliana mMDH was found acetylated on four lysines (K170, K325, K329, and K334) (König et al., 2014a), while *P. patens* mMDH was acetylated in one unique lysine (K172) of Pp3c4_20940V3.1, in the following named mMDH1, or K170 of Pp3c12_8120V3.1, in the following named mMDH2, corresponding to K169 of *A. thaliana* mMDH1 (Table 1, Figure 3). Acetylation at K170 of *A. thaliana* mMDH proteins and K172 of *P. patens* mMDH proteins could not be unequivocally assigned to one of the two paralogs, mMDH1 and mMDH2, present in each species (Figure S1). However, in the proteomic datasets of both *A. thaliana* and *P. patens*, mMDH1 was more abundant than mMDH2 (Table S1, König et al., 2014b). Hence, we focused our further analyses on the dominant mMDH protein, mMDH1, of both species.

In addition to the presence of an acetylation site, it may be argued that its occupancy (site stoichiometry) can offer some hint on the importance of the modification for protein function. To get insight into the site stoichiometry of lysine acetylation, we conducted a site stoichiometry analysis of lysine acetylation on *P. patens* proteins. We compared the peptide abundances of the modified and unmodified peptides containing K170/K172 using a dimethyl-labeling approach (Lassowskat et al., 2017). The site stoichiometry can be estimated by the assumption that in different conditions modified peptides should have their abundance changed inversely proportional to their non-modified counterpart (Olsen et al., 2010). Here we selected light- and dark-incubated samples based on the assumption that mitochondrial acetyl-CoA levels change depending on the light-controlled pyruvate dehydrogenase activity (Zhang et al., 2021), which in turn may affect mitochondrial protein acetylation (König et al., 2014a). In this analysis, relative ratios of 126 different protein acetylation sites were quantified in all three biological replicates and site occupancy levels were calculated by MaxQuant (Cox and Mann, 2008) (Table S5a). Equal labeling of peptides in all three biological replicates was observed by the equal distribution of the $\log_2$-transformed heavy/light peptide ratios around 0 (Figure S2). In total, 289 acetylation sites were quantified in at least two of the three biological replicates. A higher number
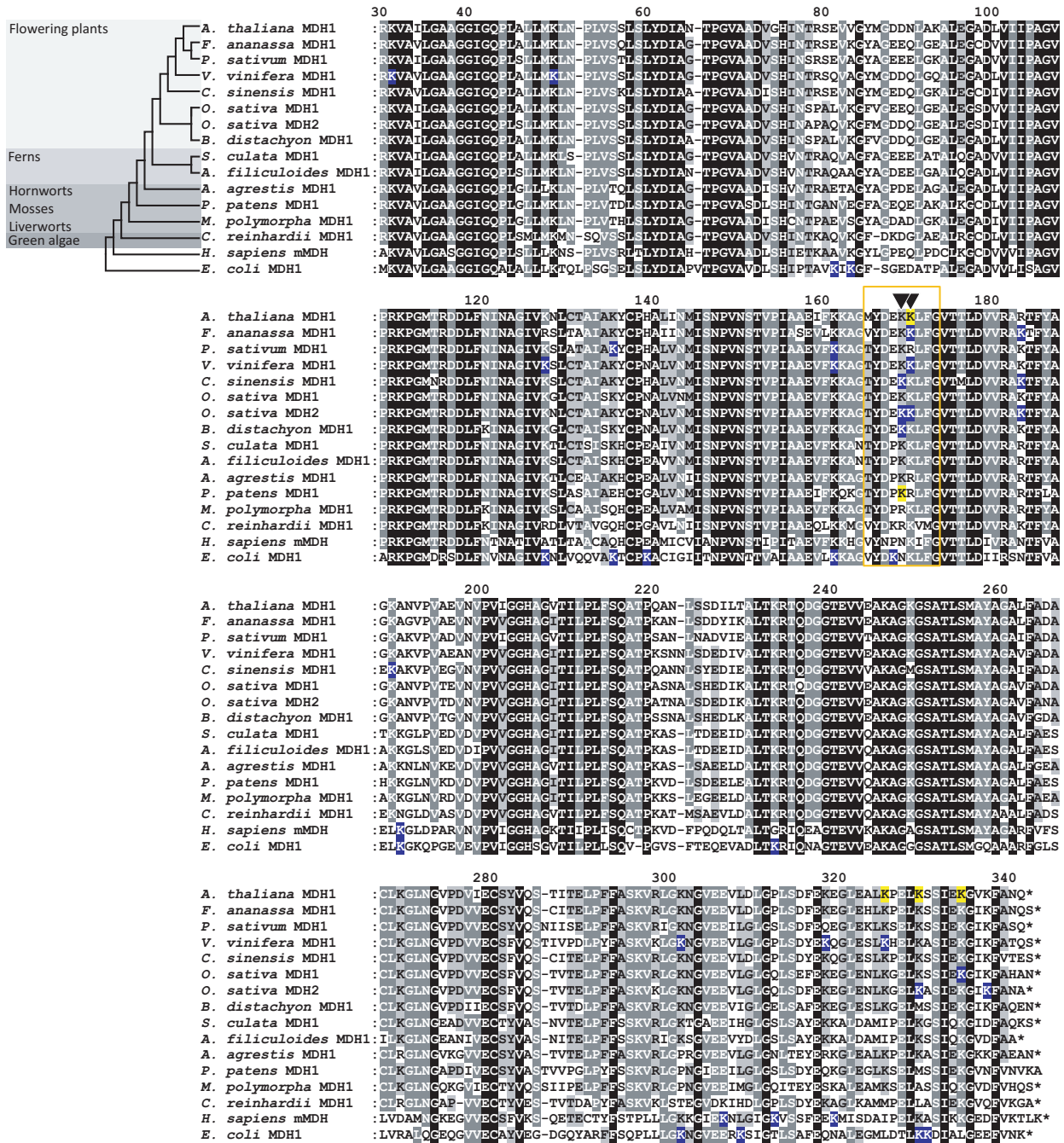
Figure 3. Sequence conservation of mitochondrial malate dehydrogenase (mMDH) of representative species of each main land plant clade, human, and *Escherichia coli* and their lysine acetylation sites. Alignment of the acetylated protein isoforms of the mMDHs of the angiosperms *Arabidopsis thaliana*, *Fragaria ananassa*, *Pisum sativum*, *Vitis vinifera*, *Camellia sinensis*, *Oryza sativa*, and *Brachypodium distachyon* with found lysine acetylation sites marked in blue. Orthologs of representative species of other major land plant clades (the ferns *Azolla filiculoides* and *Salvinia cucullata*, the hornwort *Anthoceros agrestis*, the moss *Physcomitrium patens*, the liverwort *Marchantia polymorpha*, and the green alga *Chlamydomonas reinhardtii*) share high sequence conservation. Shading in black indicates 100%, shading in dark gray indicates >80%, and shading in light gray indicates >60% amino acid identity conservation. The cladogram is based on our current understanding of land plant phylogeny (Bremer et al., 2009; Qiu et al., 2006). The sequences of *Homo sapiens* mitochondrial MDH2 and *E. coli* MDH with their identified acetylated lysines (blue) are included for comparison. The numbering is based on the sequence of MDH1 of *A. thaliana*. The alignment starts from amino acid 30, which corresponds to the start methionine of *E. coli* MDH. Yellow highlighted Ks are the acetylated lysines in *A. thaliana* and *P. patens* mMDH1 analyzed in this study. A region with acetylation sites conserved in different species is framed in orange and includes positions K169 and K170 marked with black arrows.

of lysine acetylation sites (614 lysine acetylation sites and 18 823 unmodified peptides) were detected in replicate 2 compared to replicate 1 (290 lysine acetylation sites and 17 600 unmodified peptides) and replicate 3 (226 lysine acetylation sites and 16 813 unmodified peptides) for an unknown reason. In contrast to our initial hypothesis, no major alterations in lysine acetylation site abundances were detected in dependence on the light condition (Figure S3). Still site occupancy analysis is an integrated feature in Max-Quant software, and it will report site occupancies for all peptides where the modified and unmodified protein ratios are detected. According to this, highest occupancy levels were observed for the acetylation site K387 of the Rubisco large subunit, which ranged from 12 to 74% in between the three biological replicates, and lowest occupancy levels of around 0–0.01% were observed for carbonic anhydrase K212 (Pp3c7_14450V3.3) (Table S5a). For mMDH, however, no site occupancies were reported directly by MaxQuant, and hence we had to perform a manual inspection of the data. The lysine-acetylated peptide of mMDH was detected with a reasonably high precursor ion intensity only in the second biological replicate (Table S5b). This replicate contained overall more lysine acetylation sites compared to the other two biological replicates, which we believe must have been due to an uncontrolled unknown environmental factor, which was different compared to the other two replicates (Figure S2). In replicate 2, the precursor ion of the unmodified peptide was observed at a very low intensity in the MS1 raw spectrum at the expected elution time (Table S5b, Figure S4). Taking the background MS1 precursor intensity of the unmodified peptide into account, a site occupancy of 60–70% was calculated for K170/172 in this sample (Table S5b). Since the acetylated peptide was not detected by MaxQuant in the first and third biological replicates and here only the unmodified peptide was detected, we again performed a manual inspection of the MS raw files, and observed the acetylated precursor ions at very low intensities (Figure S4). This indicates very low occupancy levels of mMDH K170/172 acetylation in replicates 1 and 3, which were not quantifiable. While we were not able to resolve the issue why acetylation occupancy of mMDH was so variable between the biological replicates, it should be noted that lysine acetylation can be highly dynamic and that even a low site stoichiometry of acetylation does not imply a lack of functionality (Baeza et al., 2020; Narita et al., 2019). Low site occupancies might be observed in cases where part of the modified proteins reside in subcomplexes, which could be metabolomes, for example. In addition, the recent work by Baeza et al. (2020) shows that lysine acetylation site occupancy can be highly dynamic after a few hours of growth factor stimulation, and they stated that most studies which looked at site occupancies were done after long-term treatments and do not show the kinetic response of this modification. Synchronized cell

cultures might be better suited to study lysine acetylation dynamics, since acetylation occupancies may be falsely assigned as low in complex unsynchronized tissue containing different cell types. In addition, a recent analysis of *Chlamydomonas* cells grown under different carbon sources showed high dynamics in cellular protein acetylation and high occupancy levels on a selected lysine of Rubisco under heterotrophic conditions (Füßl et al., 2021). Here, our data indicate that the K170/172 site of *P. patens* mMDH can be differentially acetylated *in vivo* and can reach high levels. Hence, a systematic assessment of a range of conditions needs to be carried out as part of future studies to identify the exact factors that determine *P. patens* mMDH acetylation status.

Lysine acetylation of mMDH along the phylogeny of land plants

To analyze if acetylation of mMDH is evolutionarily conserved across land plants, we inspected available acetylome datasets of nine additional flowering plant species for the presence of acetylation sites in mMDH (Table S6). In six of these species, unique acetylated peptides of mMDHs were detected (Figure 3; Figure S1, Table S6). The species with available information on mMDH acetylation cover six different orders of flowering plants (*A. thaliana*: Brassicales [König et al., 2014], strawberry [*Fragaria ananassa*]: Rosales [Fang et al., 2015], *P. sativum*: Fabales [Smith-Hammond et al., 2014], grapevine [*Vitis vinifera*]: Vitales [Melo-Braga et al., 2012], *Camellia sinensis*: Ericales [Jiang et al., 2018], rice [*Oryza sativa*] and *Brachypodium distachyon*: Poales [He et al., 2016; Xiong et al., 2016; Zhang et al., 2015; Zhen et al., 2016; Zhou et al., 2018]).

We aligned the mMDH protein sequences of these six species with mMDHs of model plants representing different main land plant clades (ferns: *Azolla filiculoides* and *Salvinia cucullata*, hornworts: *Anthoceros agrestis*, liverworts: *Marchantia polymorpha*, green algae: *Chlamydomonas reinhardtii*), including *P. patens* as model moss and *A. thaliana* as model flowering plant. Sequences were identified via BLAST using *A. thaliana* mMDH1 as a query. For selected model species, we identified MDH proteins clustering together with mMDH of *A. thaliana* and *P. patens* in phylogenetic analyses (Figure S1). Peroxisomal and chloroplastic MDHs of *A. thaliana* and *P. patens* clustered in separate clades. For comparison, we included the *Escherichia coli* MDH and human mMDH2 along with their known lysine acetylation sites (Schilling et al., 2015; Zhao et al., 2010) in the sequence alignment (Figure 3). Sequences in the alignment are clustered based on the land plant phylogeny (Bremer et al., 2009; Qiu et al., 2006). Only for *O. sativa*, different acetylation sites in both mMDH paralogs were identified, and thus both proteins were included in the alignment (He et al., 2016; Zhao et al., 2010) (Figure 3).

An interesting pattern emerges for the two neighboring lysine residues in the mMDH sequences that correspond to K169 and K170 in the *A. thaliana* sequence (Figure 3). In different studies, these lysine residues were found acetylated in mMDHs of several plant species. K172 of *P. patens* mMDH1 (corresponding to K169 of *A. thaliana*), identified with high coverage in our *P. patens* acetylome, was also acetylated in mMDH1 of *Camellia* (Jiang et al., 2018) and *Brachypodium* (Zhen et al., 2016) leaves and in mMDH2 of *O. sativa* leaves (Zhou et al., 2018). K170 of *A. thaliana* mMDH1 was also acetylated in mMDH1 of strawberry leaves (Fang et al., 2015) and grapevine exocarp (Melo-Braga et al., 2012) and in mMDH2 of *O. sativa* embryos (He et al., 2016) (Figure 3). In rice mMDH2, the lysines at position 169 and 170 were identified as differentially acetylated in different organs. The other angiosperms in this dataset showed acetylation only on one or the other lysine (Figure 3).

Interestingly, at positions corresponding to K169 and K170 in *A. thaliana*, all other investigated species show either a lysine or an arginine; the latter is similar in structure and chemical properties to the non-acetylated lysine. Even in the plastidial and peroxisomal MDHs of *A. thaliana* and *P. patens*, either a lysine or an arginine is present at these two positions (Table S4). The peroxisomal MDH1 of *A. thaliana* shares the acetylation site with mMDH1 of *P. patens* (Figure S1, Table S4; König et al., 2014a). In the *E. coli* MDH and human MDH, however, position 169 is occupied by an asparagine, which would partially mimic the constantly acetylated lysine. Other acetylated lysines in *A. thaliana* mMDH1 are K325, K329, and K334 (König et al., 2014a), each of which was found to be acetylated in at least one other angiosperm species. Acetylated K325 was detected in *V. vinifera*, while acetylated K329 and K334 were found in *O. sativa* mMDH2 and mMDH1, respectively (Figure 3). In addition, K329 was identified to be acetylated in *E. coli* MDH (Figure 3).

Enzymatic properties of site-specific acetylated *A. thaliana* and *P. patens* mMDH1 proteoforms

The conservation of lysine acetylation sites in plant mMDH (Figure 3) prompted us to investigate the influence of acetylation on the enzymatic properties of the enzyme in the model plants *A. thaliana* and *P. patens*. We selectively incorporated acetyl-lysine (acK) at lysines K170, K325, K329, and K334 of mMDH1 of *A. thaliana* (König et al., 2014a) as well as K172 of mMDH1 of *P. patens* (Table 1, Figure 3; Tables S2 and S3). The lysine acetylation was incorporated into recombinantly expressed proteins using the amber suppression system in *E. coli*, which allows the co-translational addition of *N*-acetyl-lysine in response to a stop codon at the desired positions (Neumann et al., 2008, 2009). *Arabidopsis thaliana* and *P. patens* non-modified mMDH1 and the protein versions carrying the single

acetylated lysines were expressed in *E. coli* in the presence of *N*-acetyl-lysine and nicotinamide (to inhibit the *E. coli* deacetylase CobB) and purified to homogeneity (Figure 4a). In all cases, we obtained proteins of the expected molecular masses (33.5 kDa for *A. thaliana* and 36 kDa for *P. patens*; Figure 4a). The incorporation of lysine acetylation at the desired positions of *A. thaliana* and *P. patens* mMDH1 was confirmed by LC-MS/MS (Table S7).

We next determined the *in vitro* kinetic parameters of the purified recombinant non-modified mMDH1 and the single-site acetylated versions. First, we focused on the direction of the reduction of OAA, in which case mMDH activity is needed predominantly to produce malate for its translocation to the cytosol for redox balance (Figure 1d). We found that acetylation at positions K325 and K329 in *A. thaliana* mMDH1 had no significant effects on the kinetic parameters of the enzyme. In contrast, acetylation at K334 decreased the turnover number (k_{cat}) to 64.4% of the non-modified enzyme. Acetylation at K170 decreased the turnover number to 37% while increasing the affinity for OAA (decreasing K_m) to 50% of the non-modified enzyme. The same analysis with *P. patens* mMDH1 indicated that the acetylation in K172 doubles the turnover number in comparison to the non-modified enzyme (Figure 4b), with a corresponding increase in catalytic efficiency ($k_{cat}/K_m = 23.7 \pm 3.7$ μM^{-1} sec^{-1}) compared to the non-modified enzyme ($k_{cat}/K_m = 14.8 \pm 2.3$ μM^{-1} sec^{-1}).

We further analyzed mMDH activity in its respiratory role in the TCA cycle, in which OAA is generated by oxidation of malate (Figure 1). We found that the acetylation of all analyzed single amino acid positions in *A. thaliana* mMDH1 affected the enzymatic parameters. Acetylation at position K170 reduces the affinity for malate to 65% compared to that of the non-modified enzyme (Figure 4b). As a consequence, K170 acetylation reduces the catalytic efficiency ($k_{cat}/K_m = 0.27 \pm 0.05$ μM^{-1} sec^{-1}) to 67.5% of that of the non-modified enzyme ($k_{cat}/K_m = 0.40 \pm 0.04$ μM^{-1} sec^{-1}). Acetylation at positions K325, K329, and K334 in *A. thaliana* mMDH1 reduced the turnover number to 76–79% compared to the non-modified enzyme, while increasing the affinity for malate (reduced K_m values, Figure 4b) by 15, 24, and 74%, respectively, compared to the non-modified enzyme (Figure 4b). The changes in the kinetic parameters of acetylated mMDH1 at K334 result in a threefold enhancement of the catalytic efficiency ($k_{cat}/K_m = 1.34 \pm 0.56$ μM^{-1} sec^{-1}). In contrast, the catalytic efficiencies of the other two enzymatic variants bearing acetylation at K325 ($k_{cat}/K_m = 0.37 \pm 0.05$ μM^{-1} sec^{-1}) and at K329 ($k_{cat}/K_m = 0.40 \pm 0.08$ μM^{-1} sec^{-1}) were similar to that of the non-modified enzyme. Acetylation of *P. patens* mMDH1 in K172 had no effects on the enzymatic parameters in the malate oxidation direction compared to the non-modified enzyme (Figure 4b).

Lysine residues corresponding to K172 of MDH1 of *P. patens* were also found acetylated in three angiosperm

		A. thaliana					P. patens	
		WT	AcK169	AcK170	AcK325	AcK329	AcK334	WT	AcK172
OAA → malate	K_mOAA (μM)	17 ± 7	**39 ± 8***	**9 ± 3***	20 ± 12	17 ± 4	18 ± 6	18 ± 8	23 ± 11
	(P-value)		(<0.0001)	(0.006)	(0.526)	(1.000)	(0.749)		(0.286)
	k_{cat} (s⁻¹)	548 ± 111	582 ± 12	**204 ± 33***	471 ± 208	484 ± 130	**353 ± 18***	271 ± 17	**547 ± 41***
	(P-value)		(0.375)	(<0.0001)	(0.342)	(0.278)	(<0.0001)		(<0.0001)
	k_{cat}/K_m (μM⁻¹ s⁻¹)	38.8 ± 19.0	**15 ± 6***	24.1 ± 10.6	28.4 ± 12.5	29.1 ± 3.8	24.9 ± 7.4	14.8 ± 2.3	**23.7 ± 3.7***
	(P-value)		(0.003)	(0.065)	(0.205)	(0.168)	(0.064)		(<0.0001)
malate → OAA	$K_m$malate (μM)	298 ± 9	308 ± 30	**492 ± 44***	**253 ± 14***	**226 ± 34***	**78 ± 37***	384 ± 50	354 ± 49
	(P-value)		(0.088)	(<0.0001)	(<0.0001)	(<0.0001)	(<0.0001)		(0.175)
	k_{cat} (s⁻¹)	118 ± 16	119 ± 2	132 ± 18	**94 ± 7***	**90 ± 13***	93 ± 21	107 ± 14	111 ± 23
	(P-value)		(0.855)	(0.100)	(0.001)	(0.001)	(0.068)		(0.662)
	k_{cat}/K_m (μM⁻¹ s⁻¹)	0.40 ± 0.04	0.38 ± 0.07	**0.27 ± 0.05***	0.37 ± 0.05	0.40 ± 0.08	**1.34 ± 0.56***	0.28 ± 0.08	0.32 ± 0.07
	(P-value)		(0.468)	(<0.0001)	(0.261)	(0.845)	(0.0001)		(0.343)

Figure 4. The impact of lysine acetylation on mitochondrial malate dehydrogenase (mMDH) activity.

(a) SDS-PAGE gel stained with Coomassie of the isolated recombinant non-modified (denoted as WT) and lysine-acetylated (acK) variants of *Physcomitrium patens* (*Pp*) and *Arabidopsis thaliana* (*At*) mMDH1. To the left, molecular weight markers (Spectra Multicolor Broad Range Protein Ladder; ThermoFisher Scientific, Darmstadt, Germany).

(b) Kinetics parameters of the reduction of oxaloacetate (OAA) and oxidation of malate by recombinant non-modified (denoted as WT) and acK versions of *A. thaliana* and *P. patens* mMDH1. Data were adjusted to the Michaelis–Menten equation by non-linear regression with Prism 6 (GraphPad Software). The values represent the mean ± standard deviation; n = at least three independent enzyme preparations, each measured in triplicate. * denotes values that are statistically significantly different from the corresponding WT as evaluated by the unpaired *t*-test. The *P*-values obtained are indicated in brackets under the evaluated values.

(c) Native PAGE of recombinant non-modified (WT) and lysine-acetylated (acK) variants of *P. patens* (*Pp*) and *A. thaliana* (*At*) mMDH1. The positions of the molecular weight markers (Sigma Aldrich, Darmstadt, Germany) β-amylase (200 kDa), alcohol dehydrogenase (150 kDa), and bovine serum albumin (66 kDa) are shown on the left.

species (Jiang et al., 2018; Zhen et al., 2016; Zhou et al., 2018). We further investigated the potential conserved regulatory role of this lysine residue in *A. thaliana* mMDH1. We produced the recombinant *A. thaliana* mMDH mutant acK169 (corresponding to K172 in *P. patens*) and evaluated its kinetics parameters in both directions of the reaction. We found that, similar to *P. patens*, the acetylation of Arabidopsis mMDH1 in K169 had no significant effects on the kinetic parameters of the enzyme in the malate oxidation reaction. In contrast, in the direction of the reduction of OAA, acetylation at K169 decreases the affinity of Arabidopsis mMDH1 for OAA 2.3-fold ($K_m = 39 \pm 8$ μM⁻¹; $P \leq 0.0001$), with a corresponding decrease in catalytic efficiency ($k_{cat}/K_m = 15 \pm 6$ μM⁻¹ sec⁻¹; $P = 0.0027$) compared to the non-modified enzyme (Figure 4b).

Mobility analysis of the acetylated proteins by native PAGE

The introduction of a PTM can cause changes in structural features of a protein, which can impact the kinetic properties. To analyze if the general organization of the non-modified enzymes is maintained in the single acetylated mMDH recombinant variants produced, we compared the mobility of the enzymes by native gel electrophoresis. The isolated proteins were run side-by-side on the same gel and analyzed for MDH activity.

We found that in homogeneous native PAGE, the recombinant mMDH1 of *A. thaliana* and *P. patens* are present as single bands very likely corresponding to dimers (Figure 4d). *Arabidopsis thaliana* and *P. patens* mMDH1

proteins differ slightly in their mobility, which is likely due to the differences in the molecular masses of the subunits (Figure 4a) and different gross shapes of the proteins that can be adopted in solution. The native PAGE results demonstrate that all acetylated mMDH1 versions of *A. thaliana* and *P. patens* conserved the same oligomeric arrangements observed in the non-modified proteins (Figure 4c), indicating that the detected activity changes cannot be accounted for by changes in homooligomerization.

Mapping of acetylation sites on the crystal structures of MDH

We used the crystal structures of *E. coli* MDH (PDB ID: 1EMD) and human MDH2 (PDB ID: 2DFD) to perform homology modeling of the *A. thaliana* and *P. patens* structures and to map the acetylated lysine residues analyzed in this study onto the molecular structures. Models of the *A. thaliana* and *P. patens* mMDH1 monomers, dimers, and tetramers show that the acetylated lysine residues are located in the direct vicinity of neither the active site (Figure 5a,b) nor the dimer or tetramer interfaces predicted by the constructed models (Figure 5c–f).

Superposition analysis of the monomeric structures indicates that *A. thaliana* K170, *P. patens* K172, and *E. coli* K140 are located in the same region of the 3D structure of the proteins (Figure 6a–c), suggesting conservation of the regulatory function of these lysines by acetylation. The specific spatial orientation of the lysine side chains may differ from the orientations observed in the structures of *A. thaliana* and *P. patens*, however, since the shown structures are modeled based on the crystal structures of *E. coli* and human MDH.

We also observed that *A. thaliana* mMDH1 K329 and K334, two lysine positions that are conserved in plants, are located in the same N-terminal alpha-helix as K300 and K301 of *E. coli* MDH (Figure 6b,d), with K329 of *A. thaliana* mMDH1 occupying the same special position as K300 of *E. coli* MDH (Figure 6b,d). While the effects of acetylation

Figure 5. Structures of *Arabidopsis thaliana* and *Physcomitrium patens* mitochondrial malate dehydrogenase (mMDH1) as obtained by homology modeling. Structures of *A. thaliana* (bright green; a, c, e) and *P. patens* (dark green; b, d, f) mMDH1 were modeled as monomers (a, b), dimers (b, d), and tetramers (e, f). The structures were modeled using the crystal structure of *Escherichia coli* MDH (PDB ID: 1EMD) and human MDH2 (PDB ID: 2DFD). The acetylated lysine residues of *A. thaliana* mMDH1 are shown in magenta. The acetylated lysine residue of *P. patens* mMDH1 is shown in blue. In (a, b), the ligand molecules NAD$^+$ and citrate – in brown – were manually fitted in by aligning the structure of *Homo sapiens* MDH2. Dotted lines indicate the dimer and tetramer interfaces.
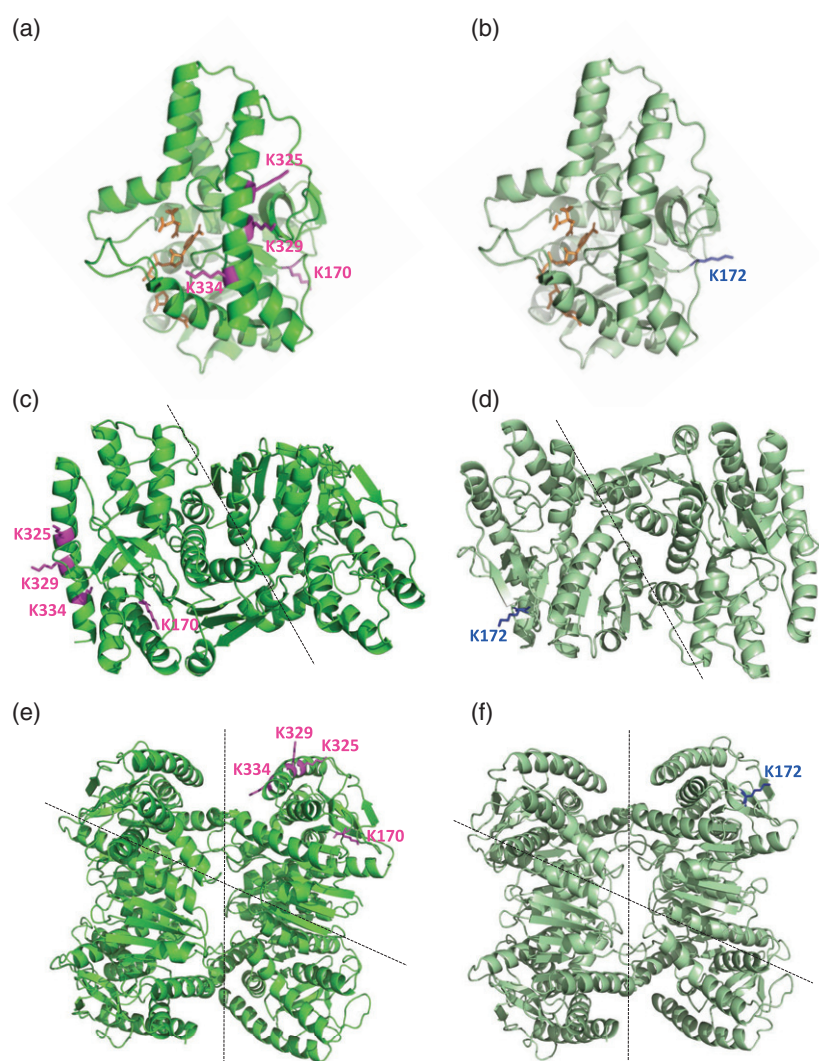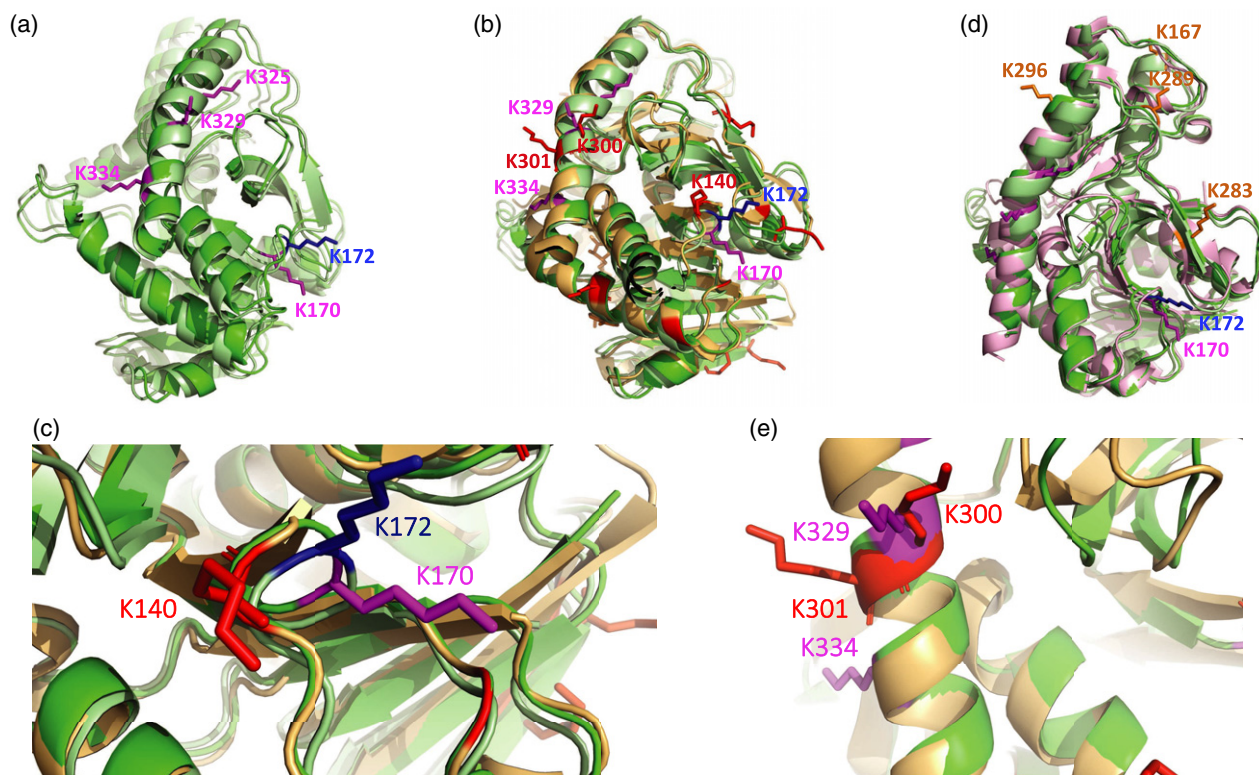
Figure 6. Superposition analysis of malate dehydrogenase (MDH) monomeric structures
(a) Structures of *Arabidopsis thaliana* (bright green-magenta) and *Physcomitrium patens* (dark green-blue) mMDH1.
(b) Structures of *A. thaliana* and *P. patens* mMDH1 and *Escherichia. coli* MDH (gold-red; PDB ID: 1EMD).
(c) Zoom in of the region containing K170 in *A. thaliana* (bright green-magenta) mMDH1, K172 in *P. patens* (dark green-blue) mMDH1, and K140 in *E. coli* (gold-red) MDH.
(d) Zoom in of the C-terminal alpha-helix containing K329 and K334 in *A. thaliana* (bright green-magenta) mMDH1 and K300 and K301 in *E. coli* (gold-red) MDH.
(e) *A. thaliana* and *P. patens* mMDH1 and human MDH2 (rose-brown; PDB ID: 2DFD). The acetylated lysine residues are shown in magenta for *A. thaliana* mMDH1, in blue for *P. patens* mMDH1, in red for *E. coli* MDH, and in brown for human MDH2. For simplicity not all lysines found to be acetylated in *E. coli* are numbered.

of K300 and K301 on the activity of *E. coli* MDH have not yet been investigated, the conserved acetylation of K300 within plants suggests a possible regulatory function.

DISCUSSION

Lysine acetylation in mitochondrial proteins of evolutionarily distant species

Acetylation of lysine residues is a particularly abundant PTM of mitochondrial and plastid proteomes (Füßl et al., 2021; Hartl et al., 2017; König et al., 2014a; Lombard et al., 2007; Smith-Hammond et al., 2014). We detected 324 lysine acetylation sites in organellar proteins of *P. patens* gametophores. Since lysine acetylation is a highly dynamic modification and its occurrence depends on the metabolic status of the organism (Meyer et al., 2018), the acetylation pattern may differ across developmental stages, organs, and growth conditions. To reduce the influence of such intra-organismic variation, we aimed at considering analogous tissues for the comparison between *A. thaliana* and

P. patens. Mitochondrial proteins were particularly over-represented amongst lysine-acetylated proteins detected in *P. patens*, even more so than in recent whole tissue acetylome studies of *A. thaliana* (Hartl et al., 2017; Uhrig et al., 2019). The number of 82 mitochondrial proteins identified here from whole *P. patens* gametophores is overall in line with 120 lysine-acetylated proteins that were detected in isolated *A. thaliana* mitochondria of seedlings (König et al., 2014a).

Due to the lack of evidence for a mitochondrial acetyl-transferase in plants, it appears likely that mitochondrial protein acetylation mostly occurs non-enzymatically between acetyl-CoA and specific lysine residues of particularly high reactivity. The functional steady-state lysine acetylation pattern is likely set by enzymatically controlled deacetylation, as carried out by sirtuin proteins (Anderson et al., 2017; König et al., 2014b; Lombard et al., 2007). In general, lysine acetylation removes the positive charge from the lysine side chains of proteins, increasing their hydrophobicity. However, similar to phosphorylation,

lysine acetylation can affect protein function in various ways, and it can cause activation as well as inhibition of enzymes depending on the function of the particular lysine residue within the protein structure (Hosp et al., 2017).

Although the same mitochondrial proteins are frequently found acetylated in different angiosperm species, the location of the particular acetylated lysines within the protein often differs (Finkemeier et al., 2011; Hosp et al., 2017). Our study shows that this is true even across land plant phylogeny. We detected the same mitochondrial proteins acetylated in the distant land plant species *P. patens* and *A. thaliana* (in total 22 orthologous protein groups were identified) and found that the majority (66%) of lysine positions that were acetylated in mitochondrial proteins of *A. thaliana* or *P. patens* was conserved in the orthologs of the other species as well (Table S4). However, even in the TCA cycle or PDC proteins, which showed high acetylation in both *P. patens* and *A. thaliana* (up to four acetylated lysines), only a low number of acetylation sites were shared (in total two) between the orthologs of the two species. A reason for the limited number of shared acetylated lysine residues detected might be the pronounced dynamics in lysine (de)acetylation, such that each experimental condition may only detect a subset of physiologically relevant acetylations. The enzymes of the TCA cycle are known to be regulated by reversible acetylation in bacterial and mammalian cells, depending on the nutritional status as well as on the circadian clock (Masri et al., 2013; Meyer et al., 2018; Wang et al., 2010). Whereas caloric restrictions generally lead to deacetylation, nutrition with sugars leads to a strong increase in mitochondrial acetylation of all TCA cycle enzymes (Meyer et al., 2018).

Lysine residues corresponding to K170 in *A. thaliana* mMDH1, for which acetylation led to changes in the enzyme catalytic parameters, were found acetylated in three other species and also under different conditions. The same was observed for site K172 of MDH1 of *P. patens*; the corresponding lysine residues were also found acetylated in three angiosperm species. The detection of homologous acetylated lysines in distant species highlights those PTMs most likely to play a physiologically relevant role in metabolic regulation.

Acetylation of lysines within a conserved hotspot modulates plant MDH activity

In addition to the identification of acetylation of *E. coli* MDH and human mMDH2 (Venkat et al., 2017), recent proteomic studies report acetylation of plant mMDH proteins, albeit in different sequence positions (Table S6). To understand the potential functional significance of mMDH acetylation, we examined the enzyme characteristics in both directions of the reversible enzymatic reaction.

Our analysis of the kinetic properties of plant mMDH1 in the OAA reduction direction indicated that lysine acetylation of K172 in *P. patens* and K169 (corresponding to K172 in *P. patens*) and K170 in *A. thaliana* have species-dependent opposite effects on the activities of the enzyme. Acetylation at K172 of *P. patens* mMDH1 enables the enzyme to convert OAA into pyruvate with a doubled catalytic rate compared with the non-modified protein. In contrast, the incorporation of an acetyl group at K169 or K170 in *A. thaliana* mMDH1 gives rise to less efficient enzymes; acetylation of K169 decreases the affinity for OAA twofold without modifying the catalytic rate, while acetylation of K170 decreases the catalytic activity by just above a third of the rate compared with the non-modified protein. A recent analysis of the protein composition of an individual average plant mitochondrion from cultured heterotrophic *A. thaliana* cells indicated that mMDH1 is highly abundant, with about 13 190 copies per mitochondrion (Fuchs et al., 2020). Adding the *in vitro* activity changes measured here to this model, the non-modified mMDH1 would have the capacity to turn over 7.2 million molecules of OAA per second in a single mitochondrion, while acetylation at K170 would reduce this conversion capacity to 2.7 million molecules per second.

We found that the turnover number of *A. thaliana* non-modified mMDH1 is twice as high as that of *P. patens* non-modified mMDH1 (Figure 4b), suggesting that the enzymes differ in their basal properties toward the substrates in the different species. These differences are likely to appear as adaptations to the metabolic environments in the species and probably result from adaptive configurations at the active site and/or of more distal regions of the proteins. Interestingly, the opposite effects of acetylation of the lysine residues in both enzymes change the turnover numbers of the acetylated proteins to values similar to those found in the non-modified enzyme of the other species analyzed: the turnover number of *P. patens* mMDH1 acetylated in K172 has a similar value to that of *A. thaliana* non-modified mMDH1, while *A. thaliana* mMDH1 acetylated in K170 has a similar turnover number to that of *P. patens* non-modified mMDH1. These observations suggest that changes of the turnover number induced by acetylation of plant mMDH1 occur between minimal and maximal values that are set by the structure and catalytic mechanism of the plant enzyme. Although the precise molecular mechanism underlying the changes in turnover number are still to be determined, it is interesting to note that amino acid 173 in *P. patens* mMDH1 (corresponding to K170 in *A. thaliana* mMDH1) is an arginine, which has similar properties as a permanently non-acetylated lysine (Kamieniarz and Schneider, 2009). Considering that the presence of an acetyl-lysine at position 170 of *A. thaliana* mMDH1 decreases the turnover number of the enzyme, the presence of an arginine in *P. patens* mMDH1 at the same position suggests that *P. patens* mMDH1 is adapted to avoid a further reduction of its enzymatic activity, at least by

acetylation. This interpretation is in accordance with the lower k_{cat} value we measured for the *P. patens* non-modified mMDH1 in comparison to that of the *A. thaliana* wild-type enzyme (Figure 4b).

The analysis of the influences of acetylation of K172 in *P. patens* and K169 and K170 in *A. thaliana* on the kinetic properties of mMDH1 in the malate oxidation direction indicated a major difference between both positions. While the kinetic properties of *P. patens* and *A. thaliana* mMDH1 acetylated at the corresponding lysine residues (K172 in *P. patens* and K169 in *A. thaliana*) were not modified, acetylation of *A. thaliana* mMDH1 at K170 reduces the enzymatic catalytic efficiency to 67.5% of that of the non-modified enzyme due to a high reduction of the affinity for malate (Figure 4b).

The lysine residues corresponding to K169 and K170 of *A. thaliana* mMDH1 that influence the enzymatic activity of *A. thaliana* and *P. patens* mMDH1 in an acetylation-dependent manner are conserved in plants and were found to be acetylated in several species. In no case the residues were found acetylated simultaneously. The fact that K169 and K170 were found to be independently acetylated in different organs (leaves and embryos) of rice may indicate the need of fine-tuning the enzyme's activity to cope with specific metabolic necessities of the organs.

Our analysis of the modeled protein structures indicates that the critical lysine residues are not near the catalytic site or in the dimer or tetramer interfaces. While the precise molecular mechanism by which acetylation influences the catalytic properties of the enzyme remains to be resolved, it appears likely that acetylation induces a conformational change that reaches across the protein structure.

Acetylation of a conserved lysine at the C-terminal end of *A. thaliana* mMDH1 favors malate oxidation activity

The C-terminus of *A. thaliana* mMDH1 contains three lysines (K325, K329, and K334) that were found acetylated in seedlings harvested at the beginning of the light period (König, 2014a). K334 is conserved in all plant species investigated in this study, while K325 and K329 are shared by approximately 80% and approximately 70% of the investigated plant species, respectively (Figure 3). The conservation of these lysine residues in plants suggests a possible conservation of their regulatory roles; yet to date, these residues were only found acetylated in mMDH orthologs of a few species beyond *A. thaliana* (Figure 3; Table S1). We found that single acetylation at K325 or K329 slightly influences the catalytic behavior of mMDH1. In contrast, acetylation at the highly conserved K334 has a major impact on the malate oxidative activity: compared to the non-modified enzyme, it decreases the catalytic efficiency of OAA to 40% while increasing the catalytic efficiency of malate oxidation 3.4-fold. A similar increase of the catalytic efficiency of the malate oxidation reaction was reported as a consequence of acetylation of MDH in other organisms. Acetylation of *E. coli* MDH at K140, which is located next to *A. thaliana* K170 and *P. patens* K172 (Figure 6c), was shown to increase the catalytic efficiency of malate oxidation 3.4-fold (Venkat et al., 2017). In the same reaction direction, the catalytic efficiency of the *E. coli* enzyme is also enhanced by acetylation of K99 (2.9-fold), while that of human mMDH2 is enhanced by acetylation of K307 (3.1-fold) (Venkat et al., 2017). However, different to Arabidopsis, the changes in catalytic efficiency observed in *E. coli* and human MDH were due to increases in enzymatic activity, while the affinity for malate was unchanged. This indicates that the activation of mMDH in different organisms involves alternative molecular mechanisms.

Potential consequences of mMDH lysine acetylation for plant metabolism

Our results indicate that acetylation of *A. thaliana* mMDH1 at the single lysine position K170 reduces the efficiency of the reaction in both directions by a similar value (67% efficiency in the OAA reduction and 72% efficiency in the malate oxidation direction). Moreover, we found that acetylation at K334 favors the malate oxidation activity of *A. thaliana* mMDH1, as it decreases the efficiency of OAA reduction while increasing the efficiency of malate oxidation. Since acetylation of K170 and K334 allows adjustments in both directions of the reaction catalyzed by mMDH1, which are fully reversible and do not require protein synthesis and/or turnover, they likely represent effective mechanisms to modulate flux through central carbon metabolism. Knowing the stoichiometry of acetylation could allow a more precise description of the impact of acetylation of a protein on metabolism (Weinert et al., 2014), even though low PTM site stoichiometry does not indicate a minor or lack of function (Bovdilova et al., 2019; Hansen et al., 2019; Xia et al., 2012). The degree of acetylation of the individual lysines analyzed here is likely to vary *in vivo* depending on conditions and importantly on the cellular context. While PTM stoichiometry in a total tissue extract is a poor predictor of *in vivo* significance, the finding that acetylation of the same conserved lysine residues occurs in different plant species, even under different conditions, is an indicator of the functional relevance of the sites.

Based on the results of the kinetic analysis of the individual acetylated sites we may form hypotheses about possible metabolic contexts in which the analyzed acetylation sites of plant mMDH may be relevant. Under conditions of high NAD^+/NADH ratio in the matrix, the activity of mMDH1 in the OAA reduction direction needs to be limited, while that in the malate oxidation direction must be boosted to avoid further removal of reductant from the matrix and constraints on mitochondrial ATP production in turn (Figure 1). Acetylation of *P. patens* mMDH1 at K172 increases the capacity – and potentially the rate – of OAA

consumption, which will be necessary under metabolic conditions that demand a high rate of matrix NAD^+ provision at the expense of ATP production, e.g., under photorespiratory conditions (Figure 1). In *E. coli*, the activity of MDH in the malate oxidation direction and the acetylation grade of the enzyme increase with increasing glucose concentrations (Venkat et al., 2017), suggesting activation of the enzyme to provide sufficient capacity for enhanced flux through the TCA cycle in its circular mode. Interestingly, bacteria grown on citrate, which favors the OAA reduction reaction of MDH, showed lower acetylation of MDH compared to those grown on glucose (Mall et al., 2018; Wang et al., 2010).

As PTMs can be strictly dependent on exact conditions, other mMDH lysine residues may also be acetylated under different growth conditions, at different times of the day, or in other tissues. Additional, systematic analyses will be required in the future for their identification. Nevertheless, as in the case of other PTMs, not all acetylated lysines necessarily modify the kinetic parameters of an enzyme, as we here observed in some cases (Figure 4b,c). Alternatively, these modifications may influence interactions with other proteins or factors that are not present in the *in vitro* setting devised here. Indeed, *in vivo* interactions between several mitochondrial proteins that were found acetylated in this study were recently reported in *A. thaliana in vivo* (Zhang et al., 2018), raising the possibility of further regulatory functions, e.g., by modulating metabolic channeling (Zhang et al., 2017, 2018).

Our finding that *P. patens* mMDH1 K170/K172 can either be nearly entirely deacetylated or reach high acetylation levels suggests that the changes in enzyme characteristics measured *in vitro* also carry significance *in vivo*. The acetylation status of mMDH is probably controlled by the mitochondrial sirtuins (Huang et al., 2010; König et al., 2014a). The specific factors that lead to favored acetylation or deacetylation deserve pinpointing in the future. Although observing pronounced differences in the occupancy of a PTM site in tissue extracts might provide evidence for its physiological significance, the reverse argument is not necessarily valid. Small differences in observable occupancy do not rule out important physiological functions since they may arise from specialization of protein functions in specific cells of tissues, and even within single cells (such as nanodomain formation into signaling complexes or metabolons by a small subset of proteins) (Narita et al., 2019; Sweetlove and Fernie, 2013; Zhang et al., 2020). In addition, a change in the modification state might lead to a gain in protein function by altering its cooperativity in multi-enzyme complexes (Hosp et al., 2017). Even if the stoichiometry of a PTM is low in all cells of the organism, this does not necessarily indicate that it is not important for regulation and signaling. Indeed, PTM-mediated changes in an enzyme's activity can

have a major impact on signaling, development, and metabolism, as demonstrated in various reports (Bovdilova et al., 2019; Xia et al., 2012). Several studies in yeast or mammalian cells showed that site stoichiometry is typically below 1% for lysine acetylation, with the exception of histone proteins and some transcriptional regulators (Hansen et al., 2019; Weinert et al., 2014, 2015a, 2015b, 2017). Yet, important functional implications have been documented for those sites in several studies (Narita et al., 2019). A recent site occupancy analysis of growth factor-stimulated MCF7 cells indicated that the site stoichiometry of the human mMDH protein HsMDH2 at K324 was particularly high, reaching 78%, while it was lowest on K185, reaching only 0.01% (Baeza et al., 2020). K324, which corresponds to acetylation site K329 of mMDH1 of *A. thaliana*, was not detected to be acetylated in liver cells (Zhao et al., 2010). A low site stoichiometry of about 0.1% was also detected for mouse mMDH2 in liver cells on K239 and K309 (Weinert et al., 2015b). Developmental and environmental factors are known to impact the abundance of PTMs to dynamically adjust metabolism to the actual needs of the cell and thus each experimental condition may only detect a subset of physiologically relevant acetylations in a given site stoichiometry. An extreme example is the light dependence of phosphorylation of metabolic enzymes, where no or full phosphorylation is detected depending on whether light is present or not (Kim et al., 2019; Zhang et al., 2021). Light- and acetate-dependent regulation of protein lysine acetylation is also reported in *Chlamydomonas*, which also affected the plastidial MDH protein and resulted in higher acetylation levels under heterotrophic conditions (Füßl et al., 2021).

Our present analysis offers intriguing insights into the functional impact of single-site modifications on the enzymatic kinetics. It further provides evidence for the degrees of potential *in vivo* regulation, which are likely key for the regulation of cellular metabolism but are not usually accounted for by standard reductionist *in vitro* analyses. Acetylation of evolutionarily conserved lysines provides a mechanism for tuning enzyme function to specific metabolic requirements. *In vivo*, the exact acetylation pattern across different lysine residues, which may dynamically change with the metabolic status of the cells, will govern the dynamic regulation of mMDH performance. Ideally, novel highly sensitive MS-based methods will become available in the future, which will enable us to assess the PTM site occupancies on proteins in single cells and organelles of certain plant tissues. Such analyses would allow the direct identification of relevant PTMs that regulate metabolic activity *in vivo*. Also, the interplay of the different modifications involved in the modulation of mMDH and the conditions that lead to the specific changes in mMDH acetylation status of evolutionarily conserved lysines remain to be investigated in the future.

EXPERIMENTAL PROCEDURES

Physcomitrium patens cultivation conditions

Physcomitrium patens (Hedw.) Bruch & Schimp. strain Gransden (Rensing et al., 2008) gametophores were cultivated on modified Knop medium plates (KH$_2$PO$_4$ [250 mg L^{-1}], KCl [250 mg L^{-1}], MgSO$_4$·7H$_2$O [250 mg L^{-1}], Ca(NO$_3$)$_2$·4H$_2$O [1000 mg L^{-1}], FeSO$_4$·7H$_2$O [12.5 mg L^{-1}], CuSO$_4$ [0.22 μM], ZnSO$_4$ [0.19 μM], H$_3$BO$_3$ [10 μM], Na$_2$MoO$_4$ [0.1 μM], MnCl$_2$ [2 μM], CoCl$_2$ [0.23 μM], and KI [0.17 μM], pH = 5.8, 1% [w/v] agar; Rudinger et al., 2011) at 2°C under long day conditions with 16 h light and 8 h darkness at a light intensity of 65 μmol m^{-2} sec^{-1} using Osram HO 39W/865 Lumilux Cool Daylight neon tubes. Single gametophores were transferred onto fresh plates 3 weeks prior to harvest and were further cultivated at 10 h light and 14 h darkness.

Trypsin digestion, immuno-enrichment of lysine-acetylated peptides, and LC-MS/MS data acquisition

The lysine acetylome analysis was performed as described in detail in Lassowskat et al. (2017). Briefly, proteins were extracted from three independent replicates (including 5–6 gametophores/plate and 9–15 plates per replicate). For quantification of acetylation site stoichiometry, digested peptides from gametophore samples harvested 30 min before and after dawn were dimethyl-labeled on C$_{18}$ Sep-Pak plus short columns (Waters) as previously described (Lassowskat et al., 2017). Equal amounts of light and medium labeled peptides were pooled for each replicate. Samples were analyzed in biological triplicates and in the second replicate the labeling was swapped to avoid any labeling bias. Protein extracts were alkylated and digested with MS-grade trypsin. Peptides were desalted and enriched for lysine-acetylated proteins by immuno-purification. Total peptide samples and the immuno-enriched fractions were then analyzed via LC-MS/MS using an EASY-nLC 1200 (Thermo Fisher) coupled to a Q Exactive HF mass spectrometer (Thermo Fisher, Schwerte, Germany). Peptides were separated on 20-cm fritless silica emitters (New Objective, 0.75 μm inner diameter), packed in-house with reversed-phase ReproSil-Pur C18 AQ 1.9 μm resin (Dr. Maisch). The column was kept at 50°C in a column oven throughout the run. The following parameters were used for acetylome analysis. Peptides were eluted for 78 min using a segmented linear gradient of 0–98% solvent B (solvent A: 0% acetonitrile [ACN], 0.1% formic acid [FA]; solvent B, 80% ACN, 0.1% FA) at a flow rate of 250 nl min^{-1}. Mass spectra were acquired in data-dependent acquisition mode with a Top12 method. MS spectra were acquired in the Orbitrap analyzer with a mass range of 300–1759 *m/z* at a resolution of 120 000 full width at half maximum (FWHM), a maximum IT of 55 msec, and a target value of 3 × 10^6 ions. Precursors were selected with an isolation window of 1.2 *m/z*. Higher-energy C-trap dissociation fragmentation was performed at a normalized collision energy of 25 eV. MS/MS spectra were acquired with a target value of 5 × 10^4 ions at a resolution of 15 000 FWHM, a maximum IT of 150 msec, and a fixed first mass of *m/z* 100. Peptides with a charge of +1, with a charge of >6, or with unassigned charge state were excluded from fragmentation for MS2, and dynamic exclusion for 30 sec prevented repeated selection of precursors.

MS data analysis

Raw data were processed using MaxQuant software V1.6.17 (http://www.maxquant.org/) (Cox and Mann, 2008). MS/MS spectra were searched with the Andromeda engine against the cosmoss_V3.3 database (February 15, 2017, https://www.cosmoss.org/physcome_

project/wiki/Downloads). Sequences of 248 common contaminant proteins and decoy sequences were automatically added during the search. Trypsin specificity was required and a maximum of four missed cleavages were allowed. Minimal peptide length was set to seven amino acids. Carbamidomethylation of cysteine residues was set as fixed, and oxidation of methionine, protein N-terminal acetylation, and acetylation of lysines were set as variable modifications. Light and medium dimethylation of lysines and peptide N-termini were set as labels. Peptide–spectrum matches and proteins were retained if they were below a false discovery rate of 1%; modified peptides were additionally filtered for a score of ≥35 and a delta score of ≥6 to remove low-quality identifications. Match between runs and requantify options were enabled. For acetylome analyses, reverse hits and contaminants were removed. Acetylation sites were filtered for a localization probability of ≥0.75. Occupancy calculations were performed using the algorithm of Olsen and co-workers within MaxQuant as well as manually (Olsen et al., 2010). Since the unmodified peptide at the lysine site K170/K172 of *P. patens* has a length of six amino acids, the MaxQuant settings were adjusted accordingly for the occupancy analyses. MS1 precursor intensities of the light and heavy labeled unmodified and acetylated MDH1 peptides were observed in all three replicates after manual inspection of the raw files (Figure S4). Due to the low signal intensities of the acetylated peptide in replicates 1 and 3 at the MS1 background threshold and the low signal intensity of the unmodified peptide in replicate 2, the MS1 precursor intensities were not detected by MaxQuant and were only visible after manual inspection with XCalibur software (Thermo-Fisher Scientific, Darmstadt, Germany) (Figure S4).

MS analyses of the recombinant mMDH proteins

The recombinant proteins (10 μg each) were alkylated and trypsin-digested in urea buffer as described previously (König et al., 2014b). Up to 500 ng of the trypsinized peptides was analyzed by LC-MS/MS as described above with the following differences. Mass spectra were acquired in data-dependent acquisition mode with a Top15 method. MS spectra were acquired in the Orbitrap analyzer with a mass range of 300–1759 *m/z* at a resolution of 60 000 FWHM, a maximum IT of 30 msec, and a target value of 3 × 10^6 ions. Precursors were selected with an isolation window of 1.3 *m/z*. MS/MS spectra were acquired with a target value of 1 × 10^5 ions at a resolution of 15 000 FWHM and a maximum IT of 55 msec. For the data analysis, MaxQuant software was used with standard settings and the following additions: MS/MS spectra were searched with the Andromeda engine against the UniProt *E. coli* K12 database including the protein sequence of either *P. patens* or *A. thaliana* mMDH. Trypsin specificity was required and a maximum of two missed cleavages were allowed. Carbamidomethylation of cysteine residues was set as fixed, and oxidation of methionine and acetylation of lysines were set as variable modifications. Results of all mMDH peptides based on a modification-specific peptide table are presented in Table S7. It has to be noted that some acetylation sites are present on the recombinant mMDH proteins due to untargeted acetylation from *E. coli*; however, these acetylation sites are only present at very low levels (mostly below 1%) as estimated from the peptide intensities compared to the unmodified peptide intensities.

Functional classification and prediction of subcellular localization

Proteins were functionally annotated based on the *P. patens* V3.3 database. Localization was inferred from the experimental dataset by Müller et al. (2014) and the GO_CC annotation provided in Lang et al. (2018).

Comparison of acetylated lysines of putative mitochondrial orthologs

Sequences of the 120 acetylated *A. thaliana* proteins identified in König et al. (2014a) were obtained from The Arabidopsis Information Resource (https://www.arabidopsis.org/tools/bulk/sequences/index.jsp) and sequences of those *P. patens* proteins that were acetylated and classified were obtained from Peatmoss (https://peatmoss.online.uni-marburg.de/ppatens_db/pp_search_input.php) (Fernandez-Pozo et al., 2020). Amino acid sequences of both species were combined and clustered using the multiple alignment program MAFFT Version 7 with default settings (Katoh et al., 2002, 2019). *Physcomitrium patens* and *A. thaliana* protein sequences of orthologous groups were aligned again with Muscle (Edgar, 2004) using MEGA 7 software (Kumar et al., 2016). In total, 22 clusters of *P. patens* and *A. thaliana* proteins were identified with homologs sharing sequence similarity higher than 40%. In each cluster different numbers of paralogous proteins of each species were included. Acetylation sites and amino acid positions of proteins of each orthologous group were compared. Acetylation sites were listed and positions were extracted from the original alignment (Table 1; Table S4, Data S1).

Phylogenetic analysis, comparison of sequence conservation and lysine acetylation patterns of mMDHs of different plant species

Published acetylome datasets were inspected for the presence of mMDH. In total 17 datasets for 10 different flowering plants were included in the analysis (Table S6). For seven flowering plant species lysine acetylation of mMDH proteins was detected. Plant tissues or organs in which these lysine acetylated mMDHs were detected are given in Table S6. Putative mMDH orthologs of these species were identified by BLAST searches using the *A. thaliana* mMDH1 protein sequence as query against the non-redundant protein database BLASTP and against the translated nucleotide database TBLASTN (Altschul et al., 1990) of different sources. Sequence data of the selected angiosperm species *C. sinensis*, *V. vinifera*, *O. sativa*, *B. distachyon*, and *F. ananassa* and the green alga *C. reinhardtii* were deposited at NCBI (www.ncbi.nlm.nih.gov) and sequence data of *P. patens* and *M. polymorpha* are deposited at Phytozome v12.0 (https://phytozome.jgi.doe.gov/pz/portal.html). For putative mMDH orthologs of *Azolla* and *Salvinia*, sequences are available in the Fernbase (www.fernbase.org). For *P. sativum* the URGI database was used as sequence source (Kreplak et al., 2019). The *Anthoceros* sequences were retrieved from the recently published *A. agrestis* Bonn v1 strain genome v1.1 (Li et al., 2020). The two to 10 best hits were downloaded for each species and aligned in the MEGA alignment explorer with the MUSCLE tool (Kumar et al., 2016; Tamura et al., 2015) followed by manual adjustment.

Amino acid sequence alignment was used to calculate a neighbor joining phylogeny with 1000 bootstraps (Poisson model, gamma distribution, partial deletion with a cutoff of 90%) including the peroxisomal (AT2G22780), plastidial (AT3G47520), and mitochondrial *A. thaliana* mMDH proteins. With a reduced dataset (Data S2), including all MDH proteins of the identified mitochondrial cluster, glyoxysomal/peroxisomal and plastid MDHs of *P. patens* and *A. thaliana*, MDH of *E. coli*, and mMDH2 of human, we constructed a maximum likelihood phylogram using IQ-tree software version 1.6.12 (Trifinopoulos et al., 2016). We applied the LG+G4 model for sequence evolution as the best fitting model identified by ModelFinder (Kalyaanamoorthy et al., 2017). We determined the confidence of each node from 1000 bootstrap

replicates with ultrafast bootstrap approximation 'UFBoot' (Hoang et al., 2018). In parallel we calculated a neighbor joining phylogeny with the same settings as described above (Figure S1). Sequences of mMDH proteins identified to be acetylated were aligned and conservation was displayed using GeneDoc software (https://genedoc.software.informer.com/2.7/).

Cloning of *A. thaliana* mMDH1 into the expression vector

The cDNA encoding the mMDH1 mature protein (without signal peptide) from *A. thaliana* (Hüdig et al., 2015) was introduced in the pCDF PylT-1 vector (SmR; *T7* promoter; *T7* terminator) (Neumann et al., 2009). This vector allows the expression of proteins fused to an N-terminal His tag for purification by Ni-NTA affinity chromatography. The mMDH cassette was obtained by PCR using primers mmdh1_GibFw and mmdh1_GibRv and cloned by Gibson assembly. The sequence of the resulting plasmid was verified by sequencing. The pCDFmdh1 vector was used as template for site-directed mutagenesis by PCR to change specific lysine codons to the amber codon, using the primers listed in Table S7. The following constructs were generated: pCDFmdh1amb170, pCDFmdh1amb325, pCDFmdh1amb329, and pCDFmdh1amb334. The incorporation of the desired nucleotide changes was confirmed by sequencing (Macrogen).

Cloning of *P. patens* mMDH1 into the expression vector

The coding sequence of mMDH1 (without signal peptide) of *P. patens* Gransden (gene Pp1s201_6V6.1) (Lang et al., 2018) was amplified with primers MfeI_PpMDH1_f and KpnI_PpMDH1_r (Table S8). The mMDH1 version with the amber codon for amino acid position 172 was generated by overlap extension PCR with internal primers (PpMDH1_KStop_f and PpMDH1_KStop_r, Table S8). The fragments were introduced into the pCDF PylT-1 vector (SmR; *T7* promoter; *T7* terminator) between restriction sites *Mfe*I and *Kpn*I (SmR; *T7* promoter; *T7* terminator) (Neumann et al., 2009) to generate N-terminally His-tagged mMDH1. The incorporation of the desired nucleotide changes was confirmed by sequencing (Macrogen).

Expression and purification of acetylated mMDHs

All pCDF PylT expression constructs carrying the mMDH1 versions with an amber codon instead of the codon for the lysine to be acetylated and those carrying the corresponding wild-type mMDH1 were transformed into *E. coli* Rosetta2 (DE3). Plasmid pBK-AcKRS3, carrying the acetyl-lysyl-tRNA synthetase (acKRS) (Neumann et al., 2008), was co-transformed with the pCDF PylT plasmids. For heterologous protein production, transformed cells were grown in 400 ml LB medium in the presence of the appropriate antibiotic in each case at 37°C and under continuous shaking to an OD_{600} of 0.4–0.6. The growth medium was supplemented with 10 mM *N'*-acetyl-lysine and 20 mM nicotinamide 30 min before induction. To induce the expression of the heterologous protein, 1 mM IPTG was added to the culture and the cells were incubated for 20 h at 30°C and under continuous shaking. The cellular culture was harvested at 6000 *g* for 15 min, and pellets were stored at −20°C until use.

For protein extraction, pellets were thawed on ice, resuspended in 20 mM Tris-HCl (pH 8.0) containing 500 mM NaCl, 5 mM imidazole, 1 mM phenylmethylsulfonyl fluoride, and a spatula tip of lysozyme, sonicated, and centrifuged at 14 000 *g* for 20 min at 4°C. The supernatant was used for protein purification by gravity flow immobilized metal ion chromatography on nickel-nitrilotriacetic acid agarose (Ni-NTA Agarose; ThermoFisher). The column was pre-equilibrated with 20 mM Tris-HCl buffer containing 500 mM NaCl and 5 mM imidazole. After loading of the

supernatant, the columns were washed in four steps with 500 mM NaCl in 20 mM Tris-HCl (pH 8.0) containing increasing concentrations of imidazole (5, 40, and 60 mM). Protein elution was performed in four steps with 500 μl of 20 mM Tris-HCl, 500 mM NaCl, and 200 mM imidazole. Finally, Vivaspin® 10K columns (Satorius, Germany, Göttingen, Germany) were used for protein concentration and buffer exchange (HEPES 50 mM, pH 7.4). The isolated recombinant proteins were analyzed by SDS-PAGE and LC-MS/MS (see above) to verify integrity and purity. The protein concentration was determined by Amido black assay (Dieckmann-Schuppert and Schnittler, 1997).

Kinetic characterization of acetylated mMDH1

MDH activity assays were carried out in a Synergy HT Biotek Plate Reader system at 25°C. OAA reduction was determined following the oxidation of NADH at 340 nm ($\epsilon = 6.2$ cm^{-1} mm^{-1}). The assay medium contained 50 mM HEPES-KOH (pH 7.5), 10 mM MgCl$_2$, 5 mM NADH, and variable concentrations of OAA in the range of 0.01–4 mM. Malate oxidation was determined following the reduction of NAD at 340 nm in assay medium containing 50 mM HEPES-KOH (pH 7.5), 10 mM MgCl$_2$, 4 mM NAD, and a variable concentration of malate in the range of 0.01–10 mM.

The reactions were started by the addition of the substrate. The kinetic constants were calculated with a minimum of three different enzyme batches each in at least triplicate determinations and adjusted to the Michaelis–Menten equation by non-linear regression with Prism 6 (GraphPad Software).

Gel electrophoresis

SDS-PAGE was performed using 14% (w/v) polyacrylamide gels according to Laemmli (1970) and the Spectra Multicolor Broad Range Protein Ladder molecular weight markers from Thermo-Fisher Scientific. Proteins were visualized by staining with Coomassie Brilliant Blue. Purified enzymes were analyzed on a non-denaturing 7% (w/v) polyacrylamide gel using the markers β-amylase (200 kDa), alcohol dehydrogenase (150 kDa), and bovine serum albumin (66 kDa) from Sigma Aldrich (Darmstadt, Germany). In-gel mMDH activity assays were performed by incubating the gels in the dark at room temperature in reaction buffer containing 50 mM K$_2$PO$_4$ (pH 7.4), 5 mM malate, 0.2 mM NAD, 0.05% (w/v) nitroblue tetrazolium, and 10 μM phenazine methosulfate as described in Hüdig et al. (2015).

Statistical analyses

Statistical analyses of the kinetic data were performed on data from at least three biological replicates, each measured at least in triplicate. To verify the statistical differences, *P*-values were determined using the unpaired *t*-test. Statistical analyses of the distribution of acetylation in organellar proteins and non-organellar proteins were performed with the chi-square test using the Excel package XLSTAT (Addinsoft).

Homology modeling of mMDH 3D structures

The 3D models of *E. coli* MDH (PDB ID: 1EMD) and *Homo sapiens* MDH2 (PDB ID: 2DFD) structures were obtained from the RSCB Protein Data Bank (https://www.rcsb.org/). Both *A. thaliana* and *P. patens* mMDH1 models were obtained by using the phyre2 protein structure prediction server (http://www.sbg.bio.ic.ac.uk/~phyre2/html/page.cgi?id=index) with the corresponding amino acid sequence as input. The ligand molecules NAD$^+$ and citrate were manually fitted in by aligning the structure of *H. sapiens* MDH2 (PDB ID: 2DFD) to the modeled structures of *A. thaliana* and *P.*

patens mMDH1. Images of the models were prepared using PyMOL v.2.4.0 by Schrödinger (https://pymol.org/).

AUTHOR CONTRIBUTIONS

IF, MS-R, and VGM conceived the project. MB, MBB, AB, MH, and LR performed biochemical studies on recombinant proteins. ME and JG generated the lysine acetylome of *P. patens*. MS-R performed phylogenetic and evolutionary conservation analyses. JE analyzed data of the stoichiometry experiment. MS, IF, MS-R, and VGM designed the experiments and analyzed the data together with other researchers. IF, MS-R, and VGM wrote the article with contributions of MS, MB, LR, and ME. VGM agrees to serve as the author responsible for contact and ensures communication.

CONFLICT OF INTEREST

The authors declare no competing interests.

DATA AVAILABILITY STATEMENT

The data underlying this article are available in the article and in its online Supporting material.

SUPPORTING INFORMATION

Additional Supporting Information may be found in the online version of this article.

Figure S1. Mitochondrial malate dehydrogenases along land plant phylogeny.

Figure S2. Histograms of light (L) and heavy (H) dimethyl-labeled lysine-acetylated peptides of all the three biological replicates of *P. patens* gametophore samples harvested before (−30 min) or after (+30 min) the onset of light.

Figure S3. Volcano plot of lysine acetylation site differences between *P. patens* gametophore samples harvested in light (+30 min) and in the dark (−30 min) containing 289 acetylation sites in two to three biological replicates.

Figure S4. MS1 precursor ion intensities of the heavy and light dimethyl-labeled lysine-acetylated (a) and unmodified (b) *P. patens* mMDH peptide containing K170/172 in all three biological replicates.

Table S1. Proteins identified in total extracts from *P. patens* gametophores which were immuno-enriched for lysine-acetylated peptides.

Table S2. Lysine-acetylated proteins identified in total extracts from *P. patens* gametophores after immuno-enrichment of lysine-acetylated peptides.

Table S3. Acetylated lysine sites.

Table S4. Conservation of lysine acetylation between mitochondrial proteins of orthologous groups identified in *A. thaliana* and *P. patens*.

Table S5. MS1-based quantitative data on the abundance of the *P. patens* mMDH1/2 peptide containing K170/K172 and the non-modified mMDH1/2 protein.

Table S6. Lysine acetylome data of mMDH proteins in plants, human, and *E. coli*.

Table S7. Unique peptides of mMDH recombinant proteins purified from *E. coli*.

Table S8. Primers used in this work.

Data S1. Protein alignment of identified orthologous groups.

Data S2. Sequence alignment of the MDH dataset for phylogenetic construction.

REFERENCES

Allfrey, V.G., Faulkner, R. & Mirsky, A.E. (1964) Acetylation and methylation of histones and their possible role in the regulation of RNA synthesis. *Proceedings of the National Academy of Sciences of the United States of America*, **51**, 786–794.

Altschul, S.F., Gish, W., Miller, W., Myers, E.W. & Lipman, D.J. (1990) Basic local alignment search tool. *Journal of Molecular Biology*, **215**, 403–410.

Anderson, K.A., Madsen, A.S., Olsen, C.A. & Hirschey, M.D. (2017) Metabolic control by sirtuins and other enzymes that sense NAD(+), NADH, or their ratio. *Biochimica et Biophysica Acta (BBA) - Bioenergetics*, **1858**, 991–998.

Baeza, J., Lawton, A.J., Fan, J., Smallegan, M.J., Lienert, I., Gandhi, T. *et al.* (2020) Revealing dynamic protein acetylation across subcellular compartments. *Journal of Proteome Research*, **19**, 2404–2418.

Bovdilova, A., Alexandre, B.M., Hoppner, A., Luis, I.M., Alvarez, C.E., Bickel, D. *et al.* (2019) Posttranslational modification of the NADP-malic enzyme involved in C4 photosynthesis modulates the enzymatic activity during the day. *The Plant Cell*, **31**, 2525–2539.

Bremer, B., Bremer, K., Chase, M., Fay, M., Reveal, J., Soltis, D. *et al.* (2009) An update of the Angiosperm Phylogeny Group classification for the orders and families of flowering plants: APG III. *Botanical Journal of the Linnean Society*, **161**, 105–121.

Choudhary, C., Weinert, B.T., Nishida, Y., Verdin, E. & Mann, M. (2014) The growing landscape of lysine acetylation links metabolism and cell signalling. *Nature Reviews Molecular Cell Biology*, **15**, 536–550.

Cox, J. & Mann, M. (2008) MaxQuant enables high peptide identification rates, individualized p.p.b.-range mass accuracies and proteome-wide protein quantification. *Nature Biotechnology*, **26**, 1367–1372.

Dieckmann-Schuppert, A. & Schnittler, H.J. (1997) A simple assay for quantification of protein in tissue sections, cell cultures, and cell homogenates, and of protein immobilized on solid surfaces. *Cell and Tissue Research*, **288**, 119–126.

Edgar, R.C. (2004) MUSCLE: multiple sequence alignment with high accuracy and high throughput. *Nucleic Acids Research*, **32**, 1792–1797.

Fang, X., Chen, W., Zhao, Y., Ruan, S., Zhang, H., Yan, C. *et al.* (2015) Global analysis of lysine acetylation in strawberry leaves. *Frontiers in Plant Science*, **6**, 739.

Fernandez-Pozo, N., Haas, F.B., Meyberg, R., Ullrich, K.K., Hiss, M., Perroud, P.F. *et al.* (2020) PEATmoss (Physcomitrella Expression Atlas Tool): a unified gene expression atlas for the model plant *Physcomitrella patens*. *The Plant Journal*, **102**, 165–177.

Finkemeier, I., Laxa, M., Miguet, L., Howden, A.J. & Sweetlove, L.J. (2011) Proteins of diverse function and subcellular location are lysine acetylated in Arabidopsis. *Plant Physiology*, **155**, 1779–1790.

Fuchs, P., Rugen, N., Carrie, C., Elsasser, M., Finkemeier, I., Giese, J. *et al.* (2020) Single organelle function and organization as estimated from Arabidopsis mitochondrial proteomics. *The Plant Journal*, **101**, 420–441.

Füßl, M., König, A.C., Eirich, J., Hartl, M., Kleinknecht, L., Bohne, A.V. *et al.* (2021) Dynamic light- and acetate-dependent regulation of the proteome and lysine acetylome of *Chlamydomonas*. *The Plant Journal*. https://doi.org/10.1111/tpj.15555

Gleason, W.B., Fu, Z., Birktoft, J. & Banaszak, L. (1994) Refined crystal structure of mitochondrial malate dehydrogenase from porcine heart and the consensus structure for dicarboxylic acid oxidoreductases. *Biochemistry*, **33**, 2078–2088.

Guan, K.L. & Xiong, Y. (2011) Regulation of intermediary metabolism by protein acetylation. *Trends in Biochemical Sciences*, **36**, 108–116.

Hanning, I. & Heldt, H.W. (1993) On the function of mitochondrial metabolism during photosynthesis in spinach (*Spinacia oleracea* L.) leaves (partitioning between respiration and export of redox equivalents and precursors for nitrate assimilation products). *Plant Physiology*, **103**, 1147–1154.

Hansen, B.K., Gupta, R., Baldus, L., Lyon, D., Narita, T., Lammers, M. *et al.* (2019) Analysis of human acetylation stoichiometry defines mechanistic constraints on protein regulation. *Nature Communications*, **10**, 1055.

Hartl, M., Fussl, M., Boersema, P.J., Jost, J.O., Kramer, K., Bakirbas, A. *et al.* (2017) Lysine acetylome profiling uncovers novel histone deacetylase substrate proteins in Arabidopsis. *Molecular Systems Biology*, **13**, 949.

He, D., Wang, Q., Li, M., Damaris, R.N., Yi, X., Cheng, Z. *et al.* (2016) Global proteome analyses of lysine acetylation and succinylation reveal the widespread involvement of both modification in metabolism in the embryo of germinating rice seed. *Journal of Proteome Research*, **15**, 879–890.

Hirschey, M.D., Shimazu, T., Huang, J.Y., Schwer, B. & Verdin, E. (2011) SIRT3 regulates mitochondrial protein acetylation and intermediary metabolism. *Cold Spring Harbor Symposia on Quantitative Biology*, **76**, 267–277.

Hoang, D.T., Chernomor, O., von Haeseler, A., Minh, B.Q. & Vinh, L.S. (2018) UFBoot2: improving the ultrafast bootstrap approximation. *Molecular Biology and Evolution*, **35**, 518–522.

Hosp, F., Lassowskat, I., Santoro, V., De Vleesschauwer, D., Fliegner, D., Redestig, H. *et al.* (2017) Lysine acetylation in mitochondria: from inventory to function. *Mitochondrion*, **33**, 58–71.

Huang, J.Y., Hirschey, M.D., Shimazu, T., Ho, L. & Verdin, E. (2010) Mitochondrial sirtuins. *Biochimica Et Biophysica Acta*, **1804**, 1645–1651.

Hüdig, M., Maier, A., Scherrers, I., Seidel, L., Jansen, E.E., Mettler-Altmann, T. *et al.* (2015) Plants possess a cyclic mitochondrial metabolic pathway similar to the mammalian metabolic repair mechanism involving malate dehydrogenase and l-2-hydroxyglutarate dehydrogenase. *Plant and Cell Physiology*, **56**, 1820–1830.

Imai, S., Armstrong, C.M., Kaeberlein, M. & Guarente, L. (2000) Transcriptional silencing and longevity protein Sir2 is an NAD-dependent histone deacetylase. *Nature*, **403**, 795–800.

Inuzuka, H., Gao, D., Finley, L.W., Yang, W., Wan, L., Fukushima, H. *et al.* (2012) Acetylation-dependent regulation of Skp2 function. *Cell*, **150**, 179–193.

Jiang, J., Gai, Z., Wang, Y., Fan, K., Sun, L., Wang, H. *et al.* (2018) Comprehensive proteome analyses of lysine acetylation in tea leaves by sensing nitrogen nutrition. *BMC Genomics*, **19**, 840.

Journet, E.P., Neuburger, M. & Douce, R. (1981) Role of glutamate-oxaloacetate transaminase and malate dehydrogenase in the regeneration of NAD for glycine oxidation by spinach leaf mitochondria. *Plant Physiology*, **67**, 467–469.

Kalyaanamoorthy, S., Minh, B.Q., Wong, T.K.F., von Haeseler, A. & Jermiin, L.S. (2017) ModelFinder: fast model selection for accurate phylogenetic estimates. *Nature Methods*, **14**, 587–589.

Kamieniarz, K. & Schneider, R. (2009) Tools to tackle protein acetylation. *Chemistry & Biology*, **16**, 1027–1029.

Katoh, K., Misawa, K., Kuma, K. & Miyata, T. (2002) MAFFT: a novel method for rapid multiple sequence alignment based on fast Fourier transform. *Nucleic Acids Research*, **30**, 3059–3066.

Katoh, K., Rozewicki, J. & Yamada, K.D. (2019) MAFFT online service: multiple sequence alignment, interactive sequence choice and visualization. *Briefings in Bioinformatics*, **20**, 1160–1166.

Kim, S.Y., Harvey, C.M., Giese, J., Lassowskat, I., Singh, V., Cavanagh, A.P. *et al.* (2019) In vivo evidence for a regulatory role of phosphorylation of Arabidopsis rubisco activase at the Thr78 site. *Proceedings of the*

National Academy of Sciences of the United States of America, **116**, 18723–18731.

König, A.C., Hartl, M., Boersema, P.J., Mann, M. & Finkemeier, I. (2014a) The mitochondrial lysine acetylome of Arabidopsis. *Mitochondrion*, **19**, 252–260.

König, A.C., Hartl, M., Pham, P.A., Laxa, M., Boersema, P.J., Orwat, A. *et al.* (2014b) The Arabidopsis class II sirtuin is a lysine deacetylase and interacts with mitochondrial energy metabolism. *Plant Physiology*, **164**, 1401–1414.

Kreplak, J., Madoui, M.A., Capal, P., Novak, P., Labadie, K., Aubert, G. *et al.* (2019) A reference genome for pea provides insight into legume genome evolution. *Nature Genetics*, **51**, 1411–1422.

Kumar, S., Stecher, G. & Tamura, K. (2016) MEGA7: molecular evolutionary genetics analysis version 7.0 for bigger datasets. *Molecular Biology and Evolution*, **33**, 1870–1874.

Laemmli, U.K. (1970) Cleavage of structural proteins during the assembly of the head of bacteriophage T4. *Nature*, **227**, 680–685.

Lang, D., Ullrich, K.K., Murat, F., Fuchs, J., Jenkins, J., Haas, F.B. *et al.* (2018) The *Physcomitrella patens* chromosome-scale assembly reveals moss genome structure and evolution. *The Plant Journal*, **93**, 515–533.

Lassowskat, I., Hartl, M., Hosp, F., Boersema, P.J., Mann, M. & Finkemeier, I. (2017) Dimethyl-labeling-based quantification of the lysine acetylome and proteome of plants. *Methods in Molecular Biology*, **1653**, 65–81.

Li, F.W., Nishiyama, T., Waller, M., Frangedakis, E., Keller, J., Li, Z. *et al.* (2020) *Anthoceros* genomes illuminate the origin of land plants and the unique biology of hornworts. *Nature Plants*, **6**, 259–272.

Lin, H., Su, X. & He, B. (2012) Protein lysine acylation and cysteine succination by intermediates of energy metabolism. *ACS Chemical Biology*, **7**, 947–960.

Lombard, D.B., Alt, F.W., Cheng, H.L., Bunkenborg, J., Streeper, R.S., Mostoslavsky, R. *et al.* (2007) Mammalian Sir2 homolog SIRT3 regulates global mitochondrial lysine acetylation. *Molecular and Cellular Biology*, **27**, 8807–8814.

Mall, A., Sobotta, J., Huber, C., Tschirner, C., Kowarschik, S., Bacnik, K. *et al.* (2018) Reversibility of citrate synthase allows autotrophic growth of a thermophilic bacterium. *Science*, **359**, 563–567.

Masri, S., Patel, V.R., Eckel-Mahan, K.L., Peleg, S., Forne, I., Ladurner, A.G. *et al.* (2013) Circadian acetylome reveals regulation of mitochondrial metabolic pathways. *Proceedings of the National Academy of Sciences of the United States of America*, **110**, 3339–3344.

Matsuzaki, H., Daitoku, H., Hatta, M., Aoyama, H., Yoshimochi, K. & Fukamizu, A. (2005) Acetylation of Foxo1 alters its DNA-binding ability and sensitivity to phosphorylation. *Proceedings of the National Academy of Sciences of the United States of America*, **102**, 11278–11283.

Maurino, V.G. & Engqvist, M.K. (2015) 2-Hydroxy acids in plant metabolism. *The Arabidopsis Book/American Society of Plant Biologists*, **13**, e0182.

Melo-Braga, M.N., Verano-Braga, T., Leon, I.R., Antonacci, D., Nogueira, F.C., Thelen, J.J. *et al.* (2012) Modulation of protein phosphorylation, N-glycosylation and Lys-acetylation in grape (*Vitis vinifera*) mesocarp and exocarp owing to *Lobesia botrana* infection. *Molecular & Cellular Proteomics: MCP*, **11**, 945–956.

Meyer, J.G., Softic, S., Basisty, N., Rardin, M.J., Verdin, E., Gibson, B.W. *et al.* (2018) Temporal dynamics of liver mitochondrial protein acetylation and succinylation and metabolites due to high fat diet and/or excess glucose or fructose. *PLoS One*, **13**, e0208973.

Moller, I.M., Igamberdiev, A.U., Bykova, N.V., Finkemeier, I., Rasmusson, A.G. & Schwarzlander, M. (2020) Matrix redox physiology governs the regulation of plant mitochondrial metabolism through posttranslational protein modifications. *The Plant Cell*, **32**, 573–594.

Müller, S.J., Lang, D., Hoernstein, S.N., Lang, E.G., Schuessele, C., Schmidt, A. *et al.* (2014) Quantitative analysis of the mitochondrial and plastid proteomes of the moss *Physcomitrella patens* reveals protein macro-compartmentation and microcompartmentation. *Plant Physiology*, **164**, 2081–2095.

Murphey, W.H., Kitto, G.B., Everse, J. & Kaplan, N. (1967) Malate dehydrogenases. I. A survey of molecular size measured by gel filtration. *Biochemistry*, **6**, 603–610.

Narita, T., Weinert, B.T. & Choudhary, C. (2019) Functions and mechanisms of non-histone protein acetylation. *Nature Reviews Molecular Cell Biology*, **20**, 156–174.

Neumann, H., Hancock, S.M., Buning, R., Routh, A., Chapman, L., Somers, J. *et al.* (2009) A method for genetically installing site-specific acetylation in recombinant histones defines the effects of H3 K56 acetylation. *Molecular Cell*, **36**, 153–163.

Neumann, H., Peak-Chew, S.Y. & Chin, J.W. (2008) Genetically encoding N (epsilon)-acetyllysine in recombinant proteins. *Nature Chemical Biology*, **4**, 232–234.

Noyes, B.E., Glatthaar, B.E., Garavelli, J.S. & Bradshaw, R.A. (1974) Structural and functional similarities between mitochondrial malate dehydrogenase and L-3-hydroxyacyl CoA dehydrogenase. *Proceedings of the National Academy of Sciences of the United States of America*, **71**, 1334–1338.

Olsen, J.V., Vermeulen, M., Santamaria, A., Kumar, C., Miller, M.L., Jensen, L.J. *et al.* (2010) Quantitative phosphoproteomics reveals widespread full phosphorylation site occupancy during mitosis. *Science Signaling*, **3**, ra3.

Qiu, Y.L., Li, L., Wang, B., Chen, Z., Knoop, V., Groth-Malonek, M. *et al.* (2006) The deepest divergences in land plants inferred from phylogenomic evidence. *Proceedings of the National Academy of Sciences of the United States of America*, **103**, 15511–15516.

Rensing, S.A., Goffinet, B., Meyberg, R., Wu, S.Z. & Bezanilla, M. (2020) The Moss *Physcomitrium* (*Physcomitrella*) *patens*: a model organism for non-seed plants. *The Plant Cell*, **32**, 1361–1376.

Rensing, S.A., Lang, D., Zimmer, A.D., Terry, A., Salamov, A., Shapiro, H. *et al.* (2008) The *Physcomitrella* genome reveals evolutionary insights into the conquest of land by plants. *Science*, **319**, 64–69.

Rudinger, M., Szovenyi, P., Rensing, S.A. & Knoop, V. (2011) Assigning DYW-type PPR proteins to RNA editing sites in the funariid mosses *Physcomitrella patens* and *Funaria hygrometrica*. *The Plant Journal*, **67**, 370–380.

Scheibe, R. (2004) Malate valves to balance cellular energy supply. *Physiologia Plantarum*, **120**, 21–26.

Scheibe, R., Backhausen, J.E., Emmerlich, V. & Holtgrefe, S. (2005) Strategies to maintain redox homeostasis during photosynthesis under changing conditions. *Journal of Experimental Botany*, **56**, 1481–1489.

Schilling, B., Christensen, D., Davis, R., Sahu, A.K., Hu, L.I., Walker-Peddakotla, A. *et al.* (2015) Protein acetylation dynamics in response to carbon overflow in *Escherichia coli*. *Molecular Microbiology*, **98**, 847–863.

Shameer, S., Ratcliffe, R.G. & Sweetlove, L.J. (2019) Leaf energy balance requires mitochondrial respiration and export of chloroplast NADPH in the light. *Plant Physiology*, **180**, 1947–1961.

Shore, J.D. & Chakrabarti, S.K. (1976) Subunit dissociation of mitochondrial malate dehydrogenase. *Biochemistry*, **15**, 875–879.

Smith-Hammond, C.L., Hoyos, E. & Miernyk, J.A. (2014) The pea seedling mitochondrial N(epsilon)-lysine acetylome. *Mitochondrion*, **19**(Pt B), 154–165.

Strotbek, C., Krinninger, S. & Frank, W. (2013) The moss *Physcomitrella patens*: methods and tools from cultivation to targeted analysis of gene function. *International Journal of Developmental Biology*, **57**, 553–564.

Sweetlove, L.J., Beard, K.F., Nunes-Nesi, A., Fernie, A.R. & Ratcliffe, R.G. (2010) Not just a circle: flux modes in the plant TCA cycle. *Trends in Plant Science*, **15**, 462–470.

Sweetlove, L.J. & Fernie, A.R. (2013) The spatial organization of metabolism within the plant cell. *Annual Review of Plant Biology*, **64**, 723–746.

Tamura, Y., Ito, A. & Cresswell, A.G. (2015) A systematic muscle model covering regions from the fast ramp stretches in the muscle fibres to the relatively slow stretches in the human triceps surae. *Computer Methods in Biomechanics and Biomedical Engineering*, **18**, 97–106.

Tomaz, T., Bagard, M., Pracharoenwattana, I., Linden, P., Lee, C.P., Carroll, A.J. *et al.* (2010) Mitochondrial malate dehydrogenase lowers leaf respiration and alters photorespiration and plant growth in Arabidopsis. *Plant Physiology*, **154**, 1143–1157.

Trifinopoulos, J., Nguyen, L.T., von Haeseler, A. & Minh, B.Q. (2016) W-IQ-TREE: a fast online phylogenetic tool for maximum likelihood analysis. *Nucleic Acids Research*, **44**, W232–W235.

Tronconi, M.A., Fahnenstich, H., Gerrard Weehler, M.C., Andreo, C.S., Flugge, U.I., Drincovich, M.F. *et al.* (2008) Arabidopsis NAD-malic enzyme functions as a homodimer and heterodimer and has a major impact on nocturnal metabolism. *Plant Physiology*, **146**, 1540–1552.

Tronconi, M.A., Hüdig, M., Schranz, M.E. & Maurino, V.G. (2020) Independent recruitment of duplicated β-subunit-coding NAD-ME genes aided the evolution of C4 photosynthesis in Cleomaceae. *Frontiers in Plant Science*, **11**. https://doi.org/10.3389/fpls.2020.572080

Uhrig, R.G., Schläpfer, P., Roschitzki, B., Hirsch-Hoffmann, M. & Gruissem, W. (2019) Diurnal changes in concerted plant protein phosphorylation and acetylation in Arabidopsis organs and seedlings. *The Plant Journal*, **99**, 176–194.

Venkat, S., Gregory, C., Sturges, J., Gan, Q. & Fan, C. (2017) Studying the lysine acetylation of malate dehydrogenase. *Journal of Molecular Biology*, **429**, 1396–1405.

Ventura, M., Mateo, F., Serratosa, J., Salaet, I., Carujo, S., Bachs, O. *et al.* (2010) Nuclear translocation of glyceraldehyde-3-phosphate dehydrogenase is regulated by acetylation. *International Journal of Biochemistry & Cell Biology*, **42**, 1672–1680.

Wang, Q., Zhang, Y., Yang, C., Xiong, H., Lin, Y., Yao, J. *et al.* (2010) Acetylation of metabolic enzymes coordinates carbon source utilization and metabolic flux. *Science*, **327**, 1004–1007.

Weinert, B.T., Iesmantavicius, V., Moustafa, T., Scholz, C., Wagner, S.A., Magnes, C. *et al.* (2014) Acetylation dynamics and stoichiometry in *Saccharomyces cerevisiae*. *Molecular Systems Biology*, **10**, 716.

Weinert, B.T., Iesmantavicius, V., Moustafa, T., Scholz, C., Wagner, S.A., Magnes, C. *et al.* (2015a) Acetylation dynamics and stoichiometry in *Saccharomyces cerevisiae*. *Molecular Systems Biology*, **11**, 833.

Weinert, B.T., Moustafa, T., Iesmantavicius, V., Zechner, R. & Choudhary, C. (2015b) Analysis of acetylation stoichiometry suggests that SIRT3 repairs nonenzymatic acetylation lesions. *EMBO Journal*, **34**, 2620–2632.

Weinert, B.T., Satpathy, S., Hansen, B.K., Lyon, D., Jensen, L.J. & Choudhary, C. (2017) Accurate quantification of site-specific acetylation stoichiometry reveals the impact of sirtuin deacetylase CobB on the *E. coli* acetylome. *Molecular & Cellular Proteomics: MCP*, **16**, 759–769.

Weinert, B.T., Wagner, S.A., Horn, H., Henriksen, P., Liu, W.R., Olsen, J.V. *et al.* (2011) Proteome-wide mapping of the *Drosophila* acetylome demonstrates a high degree of conservation of lysine acetylation. *Science Signaling*, **4**, ra48.

Xia, P., Wang, Z., Liu, X., Wu, B., Wang, J., Ward, T. *et al.* (2012) EB1 acetylation by P300/CBP-associated factor (PCAF) ensures accurate kinetochore-microtubule interactions in mitosis. *Proceedings of the National Academy of Sciences of the United States of America*, **109**, 16564–16569.

Xiong, Y., Peng, X., Cheng, Z., Liu, W. & Wang, G.L. (2016) A comprehensive catalog of the lysine-acetylation targets in rice (*Oryza sativa*) based on proteomic analyses. *Journal of Proteomics*, **138**, 20–29.

Xu, H., Zhang, J., Zeng, J., Jiang, L., Liu, E., Peng, C. *et al.* (2009) Inducible antisense suppression of glycolate oxidase reveals its strong regulation over photosynthesis in rice. *Journal of Experimental Botany*, **60**, 1799–1809.

Yang, X.J. & Seto, E. (2008) Lysine acetylation: codified crosstalk with other posttranslational modifications. *Molecular Cell*, **31**, 449–461.

Yoshida, K. & Hisabori, T. (2016) Adenine nucleotide-dependent and redox-independent control of mitochondrial malate dehydrogenase activity in *Arabidopsis thaliana*. *Biochimica et Biophysica Acta*, **1857**, 810–818.

Zhang, M., Chen, G.X., Lv, D.W., Li, X.H. & Yan, Y.M. (2015) N-linked glyco-proteome profiling of seedling leaf in *Brachypodium distachyon* L. *Journal of Proteome Research*, **14**, 1727–1738.

Zhang, Y., Beard, K.F.M., Swart, C., Bergmann, S., Krahnert, I., Nikoloski, Z. *et al.* (2017) Protein-protein interactions and metabolite channelling in the plant tricarboxylic acid cycle. *Nature Communications*, **8**, 15212.

Zhang, Y., Giese, J., Kerbler, S.M., Siemiatkowska, B., Perez de Souza, L., Alpers, J. *et al.* (2021) Two mitochondrial phosphatases, PP2c63 and Sal2, are required for posttranslational regulation of the TCA cycle in Arabidopsis. *Molecular Plant*, **14**, 1104–1118.

Zhang, Y., Sampathkumar, A., Kerber, S.M., Swart, C., Hille, C., Seerangan, K. *et al.* (2020) A moonlighting role for enzymes of glycolysis in the co-localization of mitochondria and chloroplasts. *Nature Communications*, **11**, 4509.

Zhang, Y., Swart, C., Alseekh, S., Scossa, F., Jiang, L., Obata, T. *et al.* (2018) The extra-pathway interactome of the TCA cycle: expected and unexpected metabolic interactions. *Plant Physiology*, **177**, 966–979.

Zhao, S., Xu, W., Jiang, W., Yu, W., Lin, Y., Zhang, T. *et al.* (2010) Regulation of cellular metabolism by protein lysine acetylation. *Science*, **327**, 1000–1004.

Zhen, S., Deng, X., Wang, J., Zhu, G., Cao, H., Yuan, L. *et al.* (2016) First comprehensive proteome analyses of lysine acetylation and succinylation in seedling leaves of *Brachypodium distachyon* L. *Scientific Reports*, **6**, 31576.

Zhou, H., Finkemeier, I., Guan, W., Tossounian, M.A., Wei, B., Young, D. *et al.* (2018) Oxidative stress-triggered interactions between the succinyl- and acetyl-proteomes of rice leaves. *Plant, Cell and Environment*, **41**, 1139–1153.